

# Soft-Switching, Interleaved Inverter for High Density Applications

Rachael G. Born

Thesis submitted to the faculty of the  
Virginia Polytechnic Institute and State University  
in partial fulfillment of the requirements for the degree of

Master of Science  
In  
Electrical Engineering

Jih-Sheng Lai, Chair  
Qiang Li  
Daniel Sable

September 14<sup>th</sup>, 2016  
Blacksburg, Virginia

Keywords: soft-switching, wide bandgap, DC-AC

Copyright 2016 Rachael G. Born

# Soft-Switching, Interleaved Inverter for High Density Applications

Rachael G. Born

## Abstract

Power density has become increasingly important for applications where weight and space are limited. Power density is a unique challenge requiring the latest transistor technology to push switching frequency to shrink passive filter size. Furthermore, while high efficiency is an important thermal handling strategy, it must be weighed against increases in component size. Google's Little Box Challenge shone light on these challenges in pushing the power density of a 2kW inverter. The rise in electric vehicle infrastructure and demand represents a unique application for power electronics: pushing the power handling capability and functionality of bi-directional, on-board electric vehicle chargers for faster charging while simultaneously shrinking them in size.

New wide-bandgap (WBG) devices, combined with soft-switching, now allow inverters to shrink in size by pushing to higher switching frequencies while maintaining efficiency. Classic H-Bridge topologies have limited switching frequency due to hard switching. Soft switching allows inverters to operate at higher frequency while minimizing switching loss. Concurrently, interleaving can reduce current handling stress and conduction loss better than simply paralleling two transistors.

A novel interleaved auxiliary resonant snubber for high-frequency soft-switching is introduced. The design of an auxiliary resonant snubber is discussed; this allows the main GaN MOSFETs to achieve zero voltage switching (ZVS). The auxiliary switches and SiC diodes achieve zero current switching (ZCS). This soft-switching strategy can be applied to any modulation scheme. Here, it is applied to an asymmetrical unipolar H-bridge with two high frequency legs interleaved. While soft-switching minimizes switching loss, conduction loss is simultaneously reduced for high-power applications by interleaving two high frequency legs. This topology is chosen for its conduction loss reduction and bi-directional capability.

# Soft-Switching, Interleaved Inverter for High Density Applications

Rachael G. Born

## General Audience Abstract

Electric vehicles have become a unique application for power electronics where battery chargers must both handle higher power and shrink in size and weight. The latest transistor technology allows the designer to push switching frequency, shrinking the size of components and increasing the power density. In 2014, Google's Little Box Challenge shone light on the design trade-offs of high power density design with new transistor technology for a 2kW inverter.

New semi-conductor materials now allow transistors to switch at higher frequency with less loss. To take advantage of these features, a new switching method is developed. The main power transistors are brought to zero voltage before turn-on with auxiliary switches and resonant current. Interleaving is added for better efficiency and power handling. With further control, this method could prove attractive for new, high-density power electronic designs. Applications for this include bi-directional chargers for electric vehicles in the 6kW range.

## Acknowledgements

First, I would like to express my deep appreciation to my advisor, Dr. Jih-Sheng Lai. Dr. Lai has been instrumental in opening up new avenues for me to learn and develop myself as an electrical engineer in the field of power electronics. With his guidance, I have learned far more than any classroom could teach, preparing me for a career beyond school. I would also like to thank Dr. Sable and Dr. Li for being some of the best professors I have had at Virginia Tech and for serving on my committee and providing helpful suggestions and support.

To everyone at Future Energy Electronics Center (FEEC) who mentored and befriended me, thank you for your kindness and passion. The insight and knowledge I have gained from discussions with all of you have been absolutely invaluable. For their help and support I would like to thank Lanhua Zhang, Xiaonan Zhao, Jason Dominic, Thomas LaBella, Chih-Shen Yeh, Baifeng Chen, Ben York, Nathan Kees, Eric Faraci, Seungryul Moon, Hidekazu Miwa, and Gary Kerr. I would also like to thank Mr. Curt Maxey for introducing me to the world of electrical engineering during my internship at Oak Ridge National Lab.

Finally, I would like to thank my Dad for his unerring support and encouragement throughout all of my crazy plans and all of the hurdles we have faced together.

# Table of Contents

<b>1</b>	<b>Introduction .....</b>	<b>1</b>
1.1	Level 2 EV charging .....	1
1.2	Achieving High Power Density and Google’s Little Box Challenge.....	3
1.3	Achieving Zero Voltage Switching.....	11
1.4	Goal and Scope of Thesis.....	17
<b>2</b>	<b>Inverter Operation .....</b>	<b>18</b>
2.1	ZVS Operation .....	18
<b>3</b>	<b>Design Tradeoffs and Prototype Hardware Selection.....</b>	<b>24</b>
3.1	Dead Time and the Resonant Circuit .....	24
3.2	Resonant Component Design Tradeoffs .....	26
3.3	Switching frequency.....	27
3.4	DC Bus Voltage .....	28
3.5	Auxiliary Active Component Selection .....	29
3.6	Main Switch Selection for High Frequency Legs .....	30
3.7	Challenges in Driving GaN.....	31
3.8	Main Switch Selection for Low Frequency Leg .....	34
3.9	Output Filter.....	34
<b>4</b>	<b>Design Summary.....</b>	<b>36</b>
4.1	Hardware Test Setup.....	36
4.2	Soft-switching.....	38
4.3	Power Density .....	38
4.4	Zero Crossing Issue.....	40
<b>5</b>	<b>Conclusion .....</b>	<b>45</b>
<b>6</b>	<b>Citations.....</b>	<b>46</b>

# List of Figures

Figure 1. On-board and off-board charging infrastructure. CC/CV means that batteries are charged with either constant current or constant voltage.....	3
Figure 2. Summary of FEEC Little Box Challenge Results .....	4
Figure 3. Hard switching interleaved inverter topology .....	4
Figure 4. Operation of full bridge inverter with asymmetrical unipolar modulation .....	6
Figure 5. Operation of unipolar, full-bridge inverter with synchronous rectification .....	8
Figure 6. Hard switching interleaved inverter with unipolar modulation.....	10
Figure 7. Auxiliary Resonant Snubber requires bipolar switching.....	12
Figure 8. Auxiliary Resonant Snubber with single coupled inductor .....	13
Figure 9. Auxiliary resonant snubber with two coupled inductors.....	14
Figure 10. Google Little Box Challenge Team auxiliary soft-switching design .....	15
Figure 11. In simulation, a current loop developed between the two auxiliary legs of this ZVS design .....	16
Figure 12. Proposed soft-switching interleaved inverter topology.....	18
Figure 13. Topological and timing circuit operation. ....	22
Figure 14. Output current direction and magnitude impact on natural ZVS .....	23
Figure 15. Equivalent circuit during resonant period .....	25
Figure 16. Resonant Current over high frequency leg switching period .....	29
Figure 17. Equivalent electrical configuration of Silicon Labs gate driver signal input .....	31
Figure 18. Layout for added reliability of gate drive circuit.....	31
Figure 19. Gating and Switch layout for Little Box Challenge PCB.....	32
Figure 20. Modified bootstrap circuit for GaN transistor gate voltage supply .....	33
Figure 21. Altium PC Board layout .....	37
Figure 22. Assembled prototype for testing.....	37
Figure 23. Auxiliary resonant circuit assists main switch to achieve ZVS .....	38
Figure 24. Autocad model of soft-switching interleaved inverter .....	39
Figure 25. PCB size for hard switching topology (left) and soft switching topology (right) .....	40
Figure 26. Synchronized turn-on and turn-off of gate signals at zero crossing points. ....	41
Figure 27. Zero crossing waveforms as a result of synchronized turn-on/off. ....	42

Figure 28. Modified gating waveforms at zero crossing. The yellow and red waveforms control the low frequency legs and the green and blue waveforms control the main switches of a single high frequency leg. .... 43

Figure 29. Spikes in current remain despite the simplified gating around the zero crossing ..... 43

Figure 30. Level of spiking on input and output current waveforms (bright and dark green, respectively) relative to level of current. The blue waveform is drain-source voltage of a low frequency switch and the red is the drain-source voltage of a high frequency switch. .... 44

## List of Tables

Table 1. Electric Vehicle Charging Categories.....	1
Table 2. Prototype Specifications .....	24
Table 3. Core Material Options for Resonant Inductor .....	27
Table 4. Switching frequency design tradeoffs.....	28
Table 5. Summary of prototype design.....	36

# 1 Introduction

---

Power density has become increasingly important in high-power applications such as electric vehicles, more-electric aircraft, and solar power. When space and weight are limited, design must focus on balancing both efficiency and component size.

As active components have continued to decrease in size while increasing in functionality, passive components – i.e. inductors and capacitors - have remained mostly unchanged. Reducing passive component size requires operating at higher frequencies. To push efficient inverters into switching at hundreds of kilohertz, both wide-bandgap devices and soft-switching schemes must be implemented. Wide-bandgap devices, such as GaN and SiC, offer faster turn-on and turn-off times, less turn-off loss, and a decrease in parasitic capacitance – all while shrinking package size [1].

First, an outline of several considerations in selecting a topology is presented; then, the detailed workings and control of one solution is introduced: an interleaved inverter with auxiliary resonant snubber.

## 1.1 Level 2 EV charging

Plug-in Hybrid Electric Vehicles (PHEV) and Electric Vehicles (EV) are on the cusp of becoming significant elements of world-wide auto sales. In addition to Tesla's 400,000 pre-orders for their upcoming Model 3 [2], traditional auto makers are entering the market with GM's Chevy Bolt, Nissan's extended range Leaf, and Ford's expected Model E – all of which plan to offer 200 mile range at around \$35,000 [3].

EV and PHEV batteries can be charged at a variety of a speeds, depending on the power level. These speeds are generally grouped into three categories and are described in Table 1.

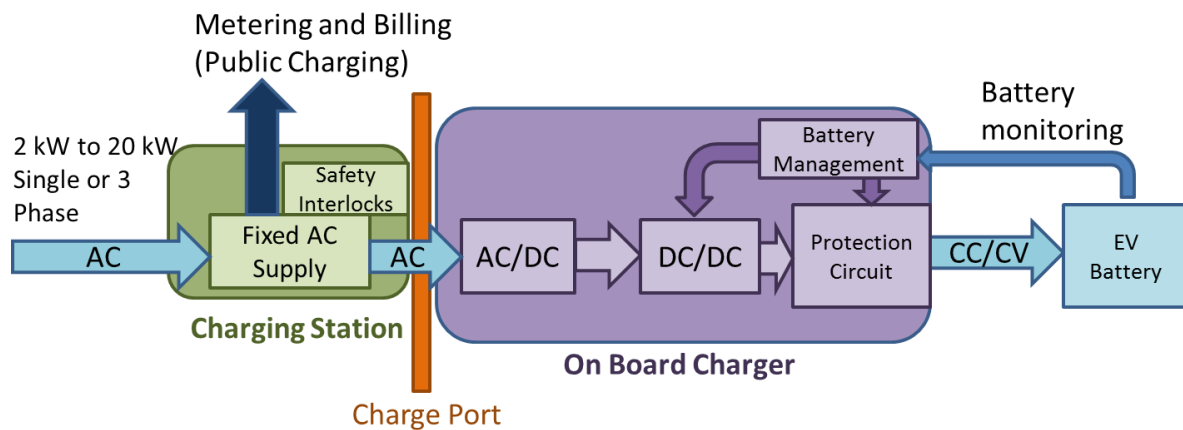
**Table 1. Electric Vehicle Charging Categories [4]**

	Supply Voltage	Power Level	Charging Speed
Level 1 Charger	120 V AC	1.2kW	2-5 miles / 1 hour of charging
Level 2 Charger	208-240 V AC	3.3kW-20kW	10-20 miles/ 1 hour of charging
DC Fast Charger	DC up to 480V	20kW – 120kW	50-70 miles/ 20 min of charging

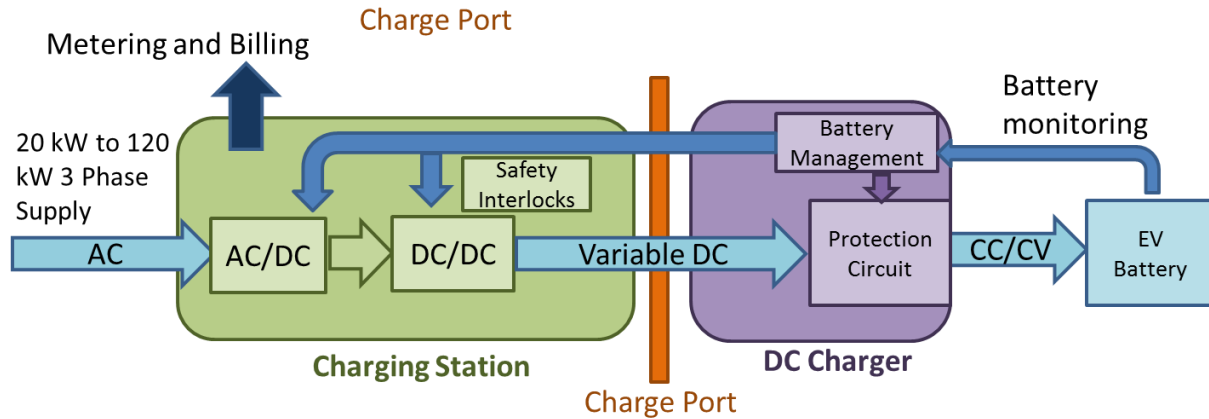
Level 1 charging is akin to plugging an electric vehicle into a normal 120V outlet at the car owner’s home or work. While slow, this method requires no extra hardware and can successfully charge a vehicle overnight. Level 2 charging can charge a vehicle in half the time as level 1 charging but requires plugging the car into a 240V outlet, though this is also commonly available in households for high-power appliances like dryers and hot water heaters. The ability to plug an electric vehicle directly into an outlet requires an on-board charger to convert the AC power of the grid to the proper DC voltage and current for battery charging. While convenient, this onboard charger consumes precious weight and space on the vehicle. Thus, level 2 charging is limited by the level of power the on-board charger can handle: 3.3kW for most PHEV’s and 6.6kW-10kW for most EV’s [5]. Without external charging equipment, charging speed is limited by the on-board charger’s power handling capability.

DC fast charging stations offer a wide range of faster charging times: from a couple of hours to a couple of minutes. The high power levels for fast charging require significant investment in a hardware off-board charger and may reduce the battery life if done regularly. These charging stations are for commercial applications to allow drivers to quickly recharge during longer road trips.

The different hardware requirements for on-board and off-board charging methods are summarized in Figure 1. While the main purpose of EV chargers is delivering power from the grid to the car batteries, bi-directional capabilities may be useful in the future for grid stabilization and even back-up power.



(a) Level 1 and 2 charging with on-board charger



(b) DC fast charging with off-board charger

**Figure 1. On-board and off-board charging infrastructure. CC/CV means that batteries are charged with either constant current or constant voltage [6]**

Because of its minimal infrastructure requirements and medium level of charging speed, Level 2 charging could become the most common form of electric vehicle charging. Increasing the power density of on-board chargers for electric vehicles could either (a) boost the power handling capability of the vehicle, increasing charging speed or (b) reduce the weight of the vehicle and/or make space for other necessary components, potentially increasing the electric driving range. Limited on-board space and weight make level 2 charging an ideal application for new advances in power-dense power electronics with wide-bandgap devices.

## 1.2 Achieving High Power Density and Google’s Little Box Challenge

Google’s Little Box Challenge [7], launched in July 2014, brought power density into the global spotlight by rewarding one million dollars to the team who could create the smallest 2kW solar inverter. In March 2016, Virginia Tech’s Future Energy Electronics Center received 3<sup>rd</sup> place with total a power density of 69W/in<sup>3</sup>, 38% more-dense than the competition’s goals. In addition to power density, Google required high efficiency, thermal management, low input ripple, minimal harmonic distortion, and electromagnetic noise mitigation. A summary of Virginia Tech’s results are shown in Figure 2.

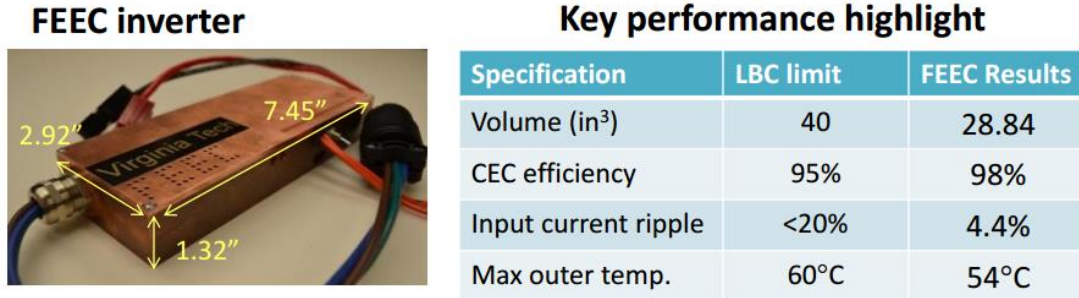


**Figure 2. Summary of FEEC Little Box Challenge Results**

To achieve these objectives, two stages were used: a DC/DC stage to control the input ripple and decrease bus voltage and a DC/AC stage to convert the input DC voltage to AC power suitable for the grid. Furthermore, wide-bandgap (WBG) devices such as Gallium Nitride (GaN) and Silicon Carbide (SiC) provided new opportunities to efficiently push power density. Mechanically, CAD software ensured full utilization of space with components selected by both electrical and form-fitting requirements. GaN switches for the DC/DC stage and DC/AC stage were directly heat-sunk to the lid and case, respectively, allowing the copper case to double as a heat sink and keeping hotter areas toward the surface for easier dissipation.

For the DC to AC stage, a high-efficiency interleaved inverter was developed to push power density in a 2kW solar inverter for Google’s little box challenge [8] as seen in Figure 3. Here, Q1-Q4 were switched at high frequency and the two legs interleaved. Q5 and Q6 were switched at line frequency. By interleaving two high frequency legs, this topology reduces current stress on the main power MOSFETs, minimizing conduction losses while shrinking output inductor size requirements. Furthermore, GaN MOSFETs eliminated reverse recovery losses during hard switching, allowing the inverter stage to reach over 99% efficiency with 60kHz switching.

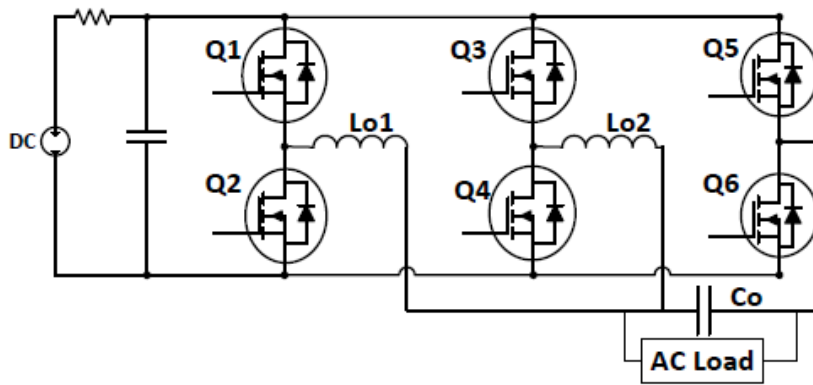
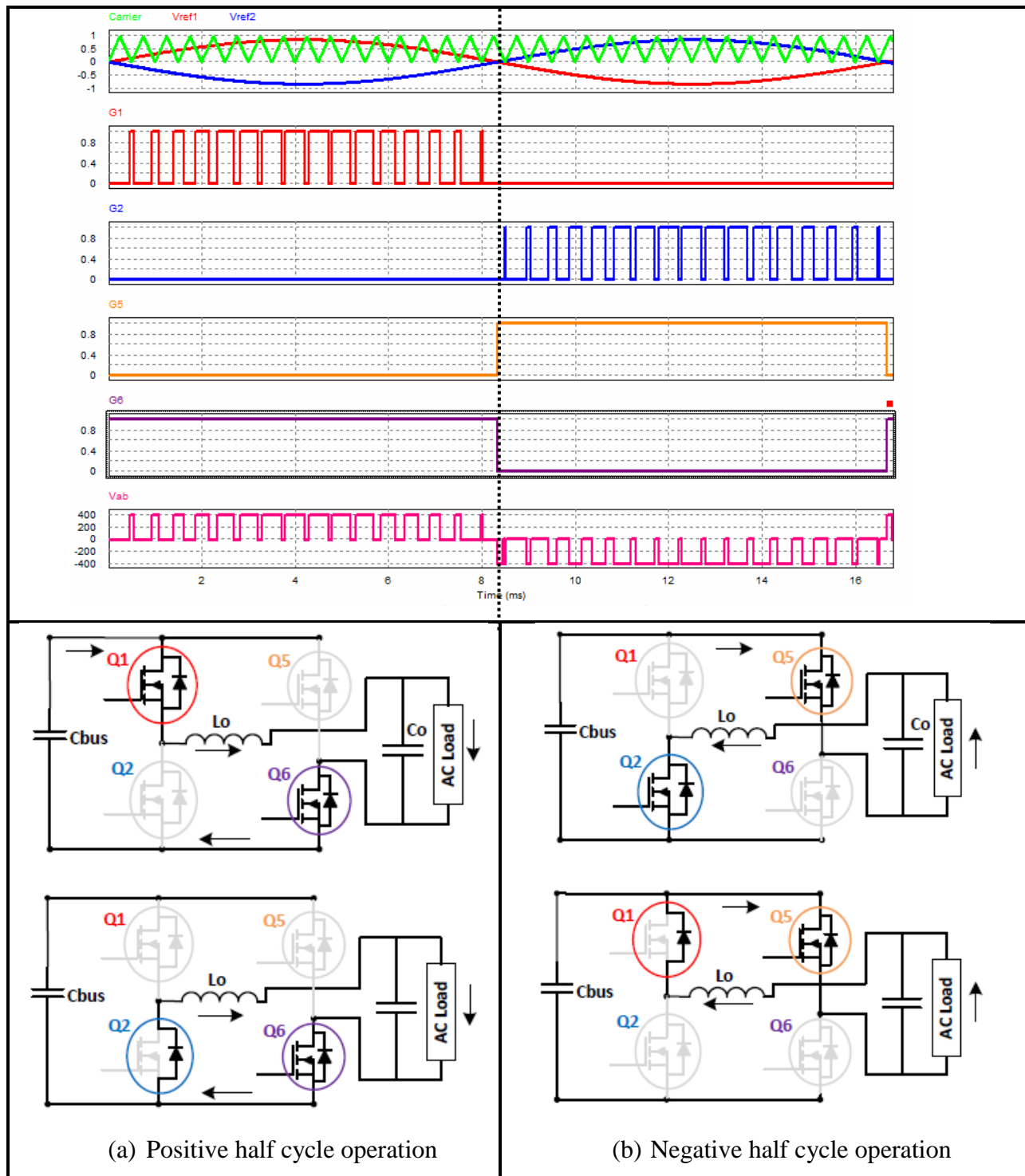


Figure 3. Hard switching interleaved inverter topology [8]

The following sections will detail the origins, benefits, and operation of the interleaved inverter.

a) **Full bridge inverter with asymmetrical unipolar modulation**

The design introduced in Figure 3 is based on a full-bridge inverter topology with asymmetrical unipolar modulation [9]. The operation of the full bridge topology is described in Figure 4. Two 60Hz reference waveforms are compared with a triangle carrier at the desired high switching frequency to produce the proper duty cycle. During the first half cycle, S1 switches at a high frequency while S3 is continuously on. When S1 is on, current travels through the MOSFET, charges the output filter inductor, and travels through S3. When S1 is off, the body diode of the bottom high frequency device (S2) conducts and the inductor discharges in a current loop. During the second half cycle, this operation is mirrored in the other two devices. S2 switches at a high frequency while S5 is continuously on. When S2 is on, current travels through S5, charges the output filter inductor, and travels through S2. When S2 is off, the body diode of the top high frequency device (S1) conducts and the inductor discharges through the current loop.



**Figure 4. Operation of full bridge inverter with asymmetrical unipolar modulation**

Because of the unipolar modulation, the voltage between the mid-point of the two legs,  $V_{ab}$ , has three levels and requires a smaller output filter than bipolar modulation.

### **a) Synchronous rectification of H-bridge**

The modulation in Figure 4 relies heavily on the MOSFET's body diode, which can have undesirable characteristics. In silicon devices, the forward drop of the body diode can be less than a volt. With GaN devices, the body diode has the advantage of zero reverse recovery charge but the disadvantage of a forward voltage drop of at least 2V – depending on the manufacturer and current level, the voltage drop could be even higher than 6V. One common way to improve the efficiency of this design is to introduce synchronous rectification. Here, instead of the body diode conducting when the partner high frequency switch is off, the MOSFET is turned on and conducts through the channel. This method can also help the inverter handle non-unity power factor loads by allowing current to flow in either the positive or negative direction if the voltage and current waveforms are out of phase. Handling non-unity power factor loads was one of the requirements of Google's Little Box Challenge and is necessary for connecting PV to the grid. It also ensures that the inverter can operate bi-directionally (given the proper control feedback) as either an inverter or rectifier. The resultant change in gate signals and operation can be seen in Figure 5.

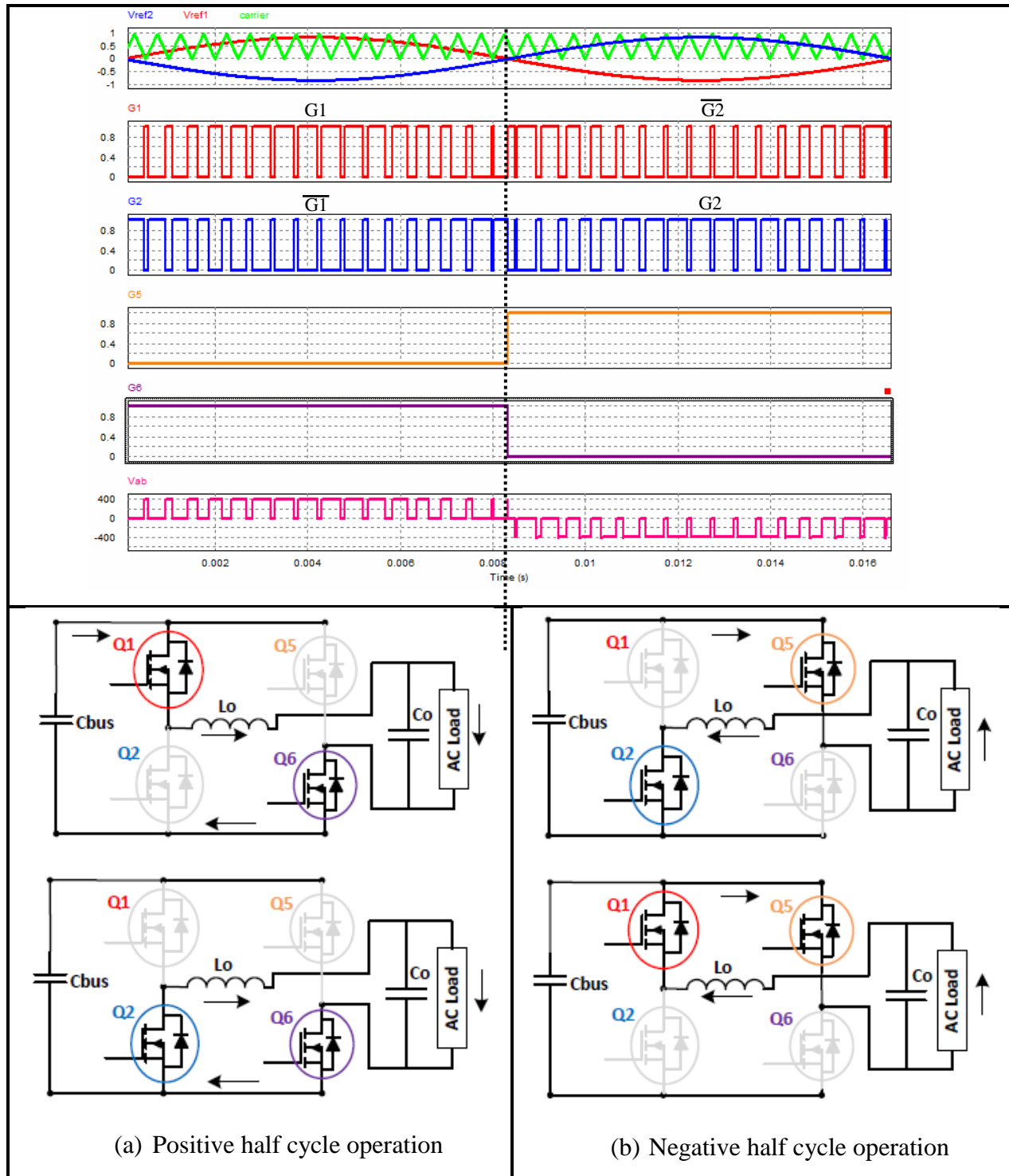


**Figure 5 Operation of unipolar, full-bridge inverter with synchronous rectification**

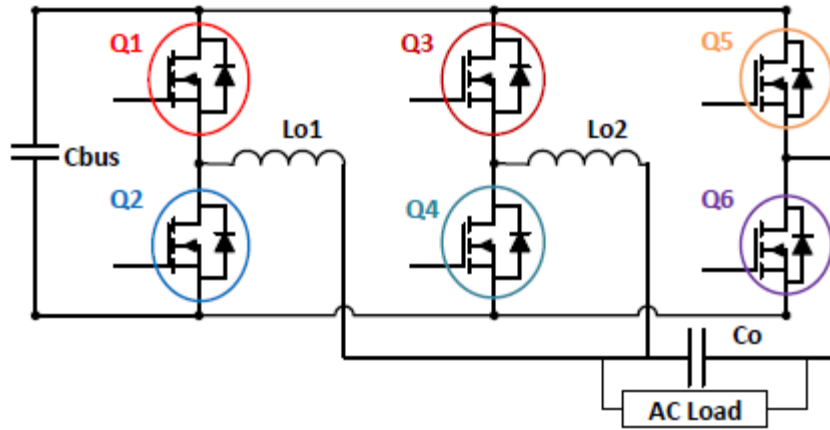
**b) Operation of hard-switching, interleaved inverter**

The final alteration to the basic H-bridge topology introduced in sections (a) and (b) to achieve the design of Figure 3 is to add a second high frequency leg. For high current

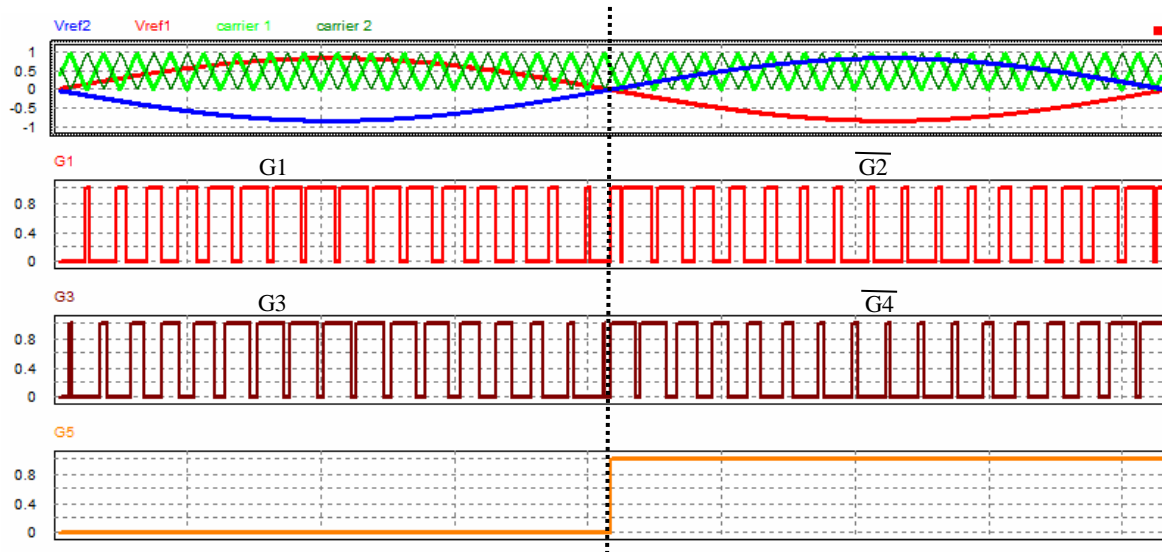
applications, it is common to parallel two MOSFETs together to share the current load and cut the conduction loss in half. While this technique reduces conduction loss in the MOSFETs themselves, it does not impact the conduction loss or size of the output filter inductor.

Interleaving two high frequency legs effectively splits the full load current between two legs, impacting not just the MOSFETs but also the output filter. Interleaving can theoretically cut the overall MOSFET conduction loss in half and the overall filter inductor conduction loss in half. The filter inductor wire can also be sized to handle a smaller current, allowing for the use of two smaller inductors instead of one large one and potentially shrinking the overall volume of the inductors. Furthermore, to interleave the two legs, the triangle carriers for the two high frequency legs are placed 180 degrees apart. The ripple on the two output current waveforms is also 180 degrees out of phase and cancels each other, further reducing output filter size requirements.

Thus, when compared with just paralleling two devices, interleaving offers better efficiency and a reduced output filter size with no additional components. Operation of the inverter with two interleaved high frequency legs and synchronous rectification is summarized in Figure 6.



(a) Interleaved inverter topology



(b) Modulation waveforms for interleaved inverter topology with unipolar modulation.

The three PWM signals control the top switch for the two high frequency legs (red for S1 and dark red for S3) and the top switch of the low frequency leg (S5 in orange).

**Figure 6. Hard switching interleaved inverter with unipolar modulation**

Google's Little Box Challenge (LBC) pushed the power density for a 2kW solar inverter, which is about the power level required for a typical home PV installation of eight panels. Yet the volume of solar panels themselves and decreasing solar power system costs make the power density of the inverter itself less of a critical factor. Yet, lessons from the LBC can be applied to an area where weight and volume are critical: on-board electric vehicle charging.

Many of the most successful entries to the LBC employed soft switching to push switching frequency to hundreds of kHz and bring power density to over  $100\text{W}/\text{in}^3$ . One advantage of GaN devices is that, compared with silicon devices with similar current handling capability, package size can be reduced. This minimizes the drain-source capacitance, speeding up turn-on and turn-off time, and allowing the MOSFET to switch at  $>100\text{MHz}$ , according to one manufacturer's data sheet. Thus, with the introduced hard switching interleaved topology serving as a foundation, this paper seeks to find a soft-switching solution that can push switching frequency from  $60\text{kHz}$  to hundreds of kHz, shrinking the output filter size of  $L_1$ ,  $L_2$ , and  $C_o$  of Figure 3 .

### **1.3 Achieving Zero Voltage Switching**

Soft switching involves bringing a device to either zero voltage or zero current before turning it on and off, theoretically eliminating switching losses [10]. This switching scheme can be achieved through either (a) a variety of precise control methods [11]-[12] or (b) additional auxiliary hardware components to drain voltage away from the switch. Control methods achieve ZVS and/or ZCS by controlling the inductor current to go through zero in every switching cycle. However, these methods require more complex control. This pushes the precision limit and response time of digital controllers and sensors, especially when implemented at high frequencies. Furthermore, because of the variable frequency, these methods increase the output current ripple and can require bigger harmonic filters.

Yet, implementing soft-switching with hardware solutions requires extra components that have their own losses and consume space. The following sections will weigh those trade-offs and discuss the origins, benefits, and design of several soft-switching topologies. Operation of the final topology chosen is discussed in section 2.

#### **a) Auxiliary Resonant Snubber**

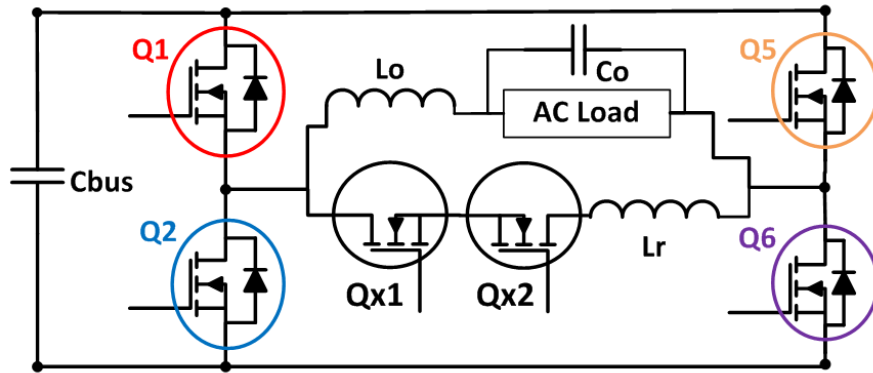


**Figure 7. Auxiliary Resonant Snubber requires bipolar switching**

The resonant snubber [13-15] in Figure 7 was attractive due to the small number of additional components. Here, the main H-bridge switches of S1, S2, S5, and S6 are supplemented with two auxiliary switches, Sx1 and Sx2, two clamping diodes (these are optional and not pictured), and a resonant inductor. The main switches use bipolar modulation where S1 and S6 are turned on/off together and S2/S5 are turned on/off together. During dead time when all four main switches are off, the auxiliary inductor resonates with the drain-source capacitance of the main switches. When this resonant current becomes larger than the load current, the voltage is charged across one pair of MOSFETs (e.g. Q2 and Q5) and drained from the other pair (e.g. Q1 and Q6), allowing Q1 and Q6 to turn on under zero voltage. Because the resonant circuit only operates during dead time, rms current of the snubber remains much smaller than within the main power circuit. Unfortunately, this auxiliary circuit requires the main switch pairs turn on and off together to reset the resonant snubber inductor current. Interleaving two high frequency legs will require unipolar modulation where the main switches of Figure 6 turn on and off at different moments.

**b) Auxiliary Resonant Snubber with coupled magnetic reset**

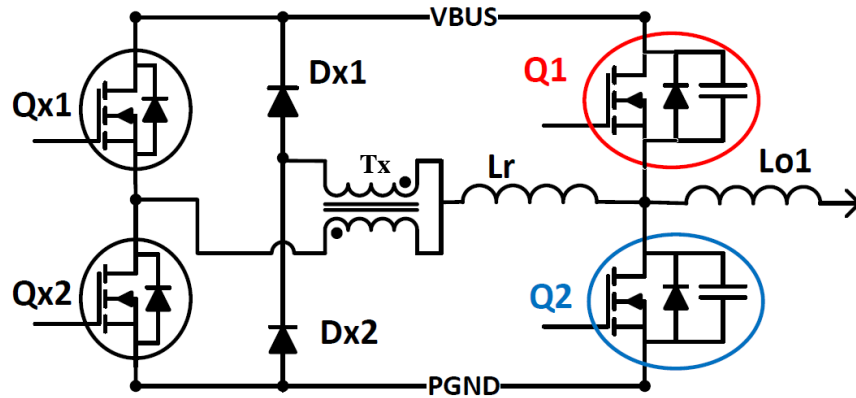


**Figure 8. Auxiliary Resonant Snubber with single coupled inductor [16]**

Unlike Figure 7 where all four main switches of an H-bridge are shown, the auxiliary resonant snubber with coupled magnetic reset [16-19] achieves ZVS for a single inverter leg. Figure 8 shows two main transistors, S1 and S2, and additional auxiliary components of two transistors, Sx1 and Sx2, four diodes, and a transformer whose leakage inductance serves as the resonant inductor. Originally, one half of the H-bridge of Figure 7 (Q5 and Q6) were replaced with two capacitors to provide a reset for the resonant current. This split capacitor solution, called auxiliary resonant commutated pole (ARCP), suffered from voltage balancing issues that complicated control. The topology of Figure 8 eliminates the split capacitance and adds a transformer to increase the forcing voltage for resonance. ZVS is achieved by turning on an auxiliary switch, charging the transformer and leakage resonant inductance to the load current. Next, the transformer leakage inductance resonates with the drain-source capacitance of the main devices and charges one drain-source capacitor to bus voltage while discharging the other one before the main switch is turned on at zero voltage. Thus, in this topology the two auxiliary switches provide a means of charging the secondary side of the transformer and resonant inductance while the four diodes handle the primary side transformer current.

**c) Auxiliary Resonant Snubber with two coupled inductors**

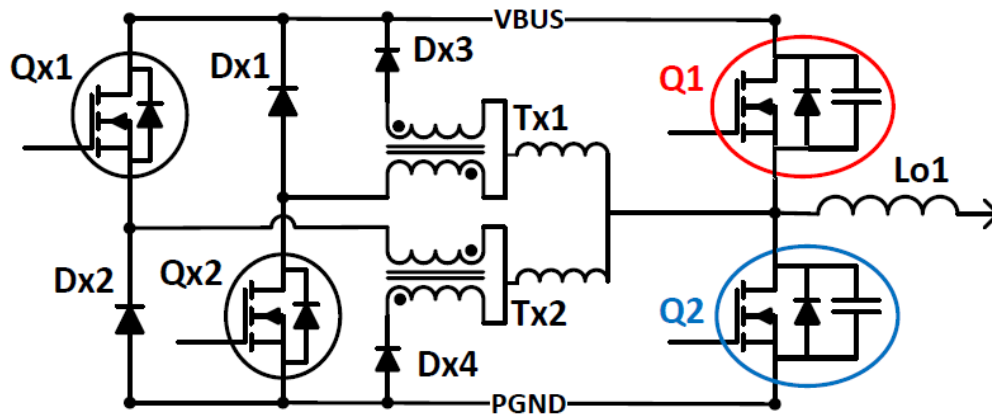


**Figure 9 Auxiliary resonant snubber with two coupled inductors [20]**

One problem with the auxiliary resonant snubber with one coupled inductor, resulting in the proposal of the topology in Figure 9, is that if the magnetizing current is not fully reset the transformer core may saturate. The auxiliary resonant snubber with two coupled magnetics [20, 21] solves this issue by implementing two coupled inductors for faster and more reliable magnetizing current reset. As in the single transformer configuration, the two auxiliary switches drive the resonance while four diodes conduct the primary side of the transformer. This configuration has been demonstrated to be highly reliable and efficient, demonstrating in [20] over 99% CEC efficiency for a 4kW PV application.

While pushing to higher frequencies reduces the output filter size, the size of the auxiliary elements is related to dead time and will add to the overall size of the inverter regardless of switching frequency. Thus, the additional size of auxiliary components must be weighed against any size reduction achieved by reaching higher frequencies. Topology (c) is both efficient and reliable at low frequencies. However, the resonant inductance of the auxiliary resonant snubber with either single or double transformers is generated by the leakage inductance of the transformer. To generate enough leakage inductance for resonance, magnetizing inductance must be significantly larger. With higher switching frequencies, the two transformers do not change in size and can become much larger than the output filter inductor.

**d) Little Box Challenge AMR team**

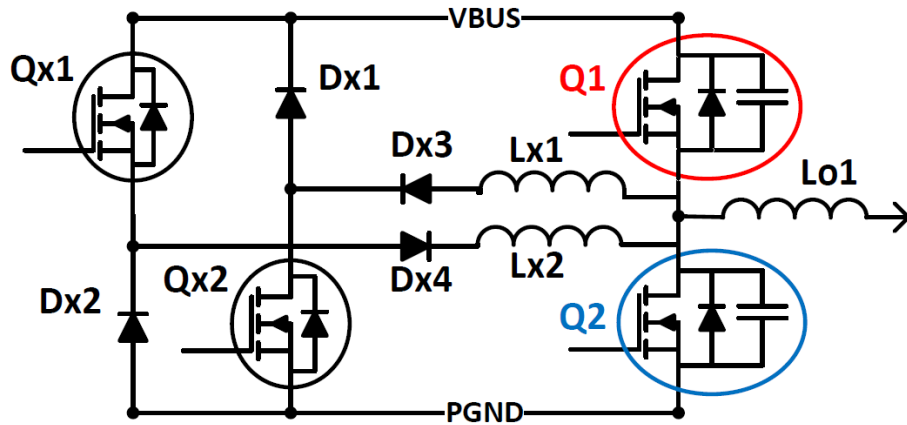
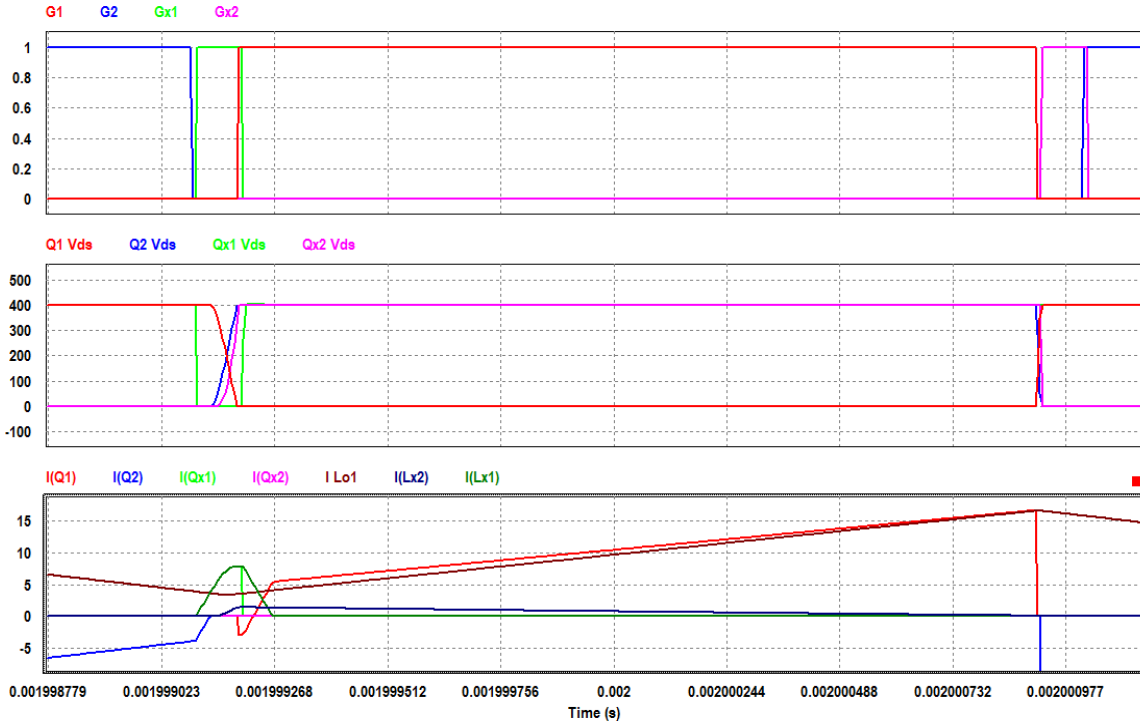


**Figure 10. Google Little Box Challenge Team auxiliary soft-switching design**

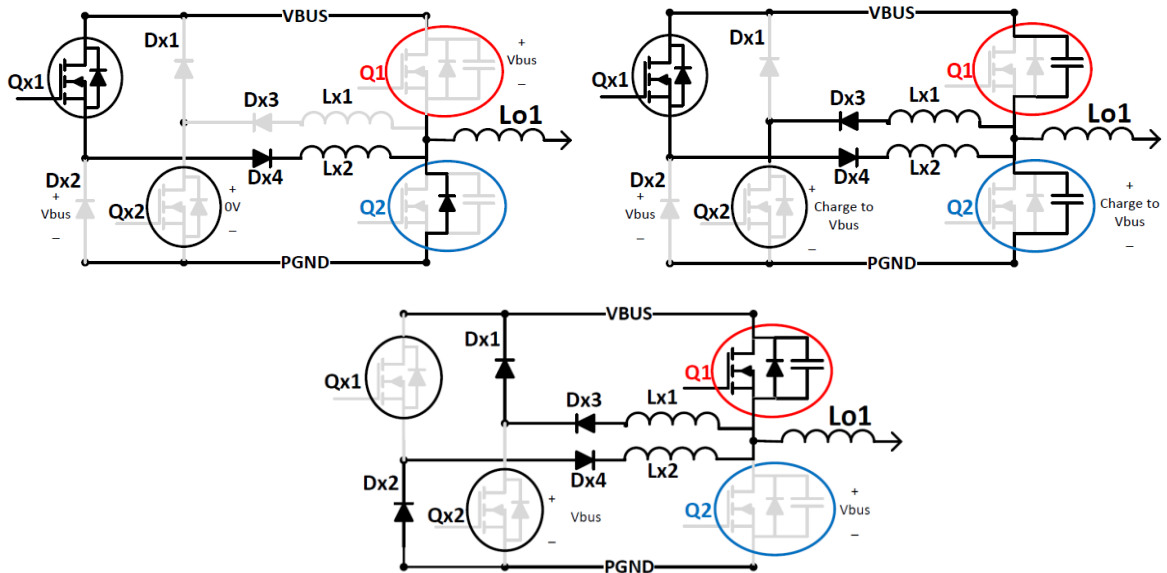
The AMR team of the little box challenge [22] came up with a dc-dc converter topology that eliminates the large transformer that plagued the power density of the topologies introduced in (b) and (c). Instead, smaller inductors are directly used for resonance. Although the passive component size is decreased, the total number of auxiliary components remain unchanged: two transistors, 4 diodes, and two inductors.

Another advantage of the topology in Figure 10 is that the resonant current should only be present during dead time. This reduces conduction loss and eliminates the worry of magnetic current reset timing. The auxiliary resonant snubber with coupled inductors in sections (b) and (c) allowed resonant current to flow during both dead time and normal operation, forcing current reset to occur quickly within the dead time.

Yet, in simulations of Figure 10 it was found that the resonant current never returned to zero and continued to circulate beyond the dead time. This could increase the rms current and losses in the auxiliary circuit. As shown in Figure 11, during dead time if the top auxiliary switch Qx1 is turned on, D4 blocks the full bus voltage and the inductor current of L2 begins to charge to the load current. During resonance, when auxiliary current surpasses output current, some current also begins to flow through L1 and D2, charging Qx2 from zero to the bus voltage at the same time Q2 is being charged. Even after Q1 turns on under ZVS, the two auxiliary inductors are still charged and continue to circulate current through a loop where the voltage across Qx1 and Qx2 is slightly larger than the voltage across Q2, according to the simulation results.



(a) Simulation waveform shows unwanted current continues to flow in auxiliary circuit outside of dead time. The dark blue waveform of  $I(Lx2)$  begins conducting current during the resonant period even though the current through  $I(Lx1)$  is the only assistant current needed for ZVS. During normal operation after dead time, as the output current (brown  $I Lo1$ ) begins to ramp up, the current through  $I(Q1)$  remains larger to supply both the output and unwanted current loop



(b) Circuit diagram of unwanted current loop

Figure 11. Current loop between the two auxiliary legs of this ZVS design allowed current to flow through auxiliary circuit beyond dead time.

To prevent this, two inductors are reduced to one and D2 and D3 become linked. Now, when Qx1 is turned on, D4 and Qx2 immediately block the bus voltage. Furthermore, during resonance current can only flow through the inductor in one direction, preventing the unwanted current loop from developing. Paring two auxiliary inductors down to one further reduces the size of this ZVS method. The single auxiliary inductor does not conduct twice as much current, but rather is used for ZVS for the entire 60Hz cycle rather than for half a cycle. A more detailed discussion of circuit operation will be held in Section 2.

## **1.4 Goal and Scope of Thesis**

The goal of this thesis is to push the power density of the inverter stage of a level two, on-board electric vehicle charger.

While Figure 1 shows the flow of power of an on-board electric vehicle charger in one direction (from the grid to the battery) research is increasingly looking toward bi-directional electric vehicle chargers to provide power to the future smart grid in peak demand moments. Here, for ease in comparison to the previously developed hard-switching inverter (described in section 1.2), this topology is tested as an inverter. Because the topology can handle bi-directional power flow, future control loop design will allow it to operate as a traditional rectifier. As a rectifier, “asymmetrical unipolar” modulation (discussed in section 1.2 part a) is more commonly referred to as a “totem pole PFC”.

The scope of this thesis is to prove the functionality of a novel soft-switching method by designing, simulating, building, and testing an inverter prototype. This soft switching method can be used on any half bridge leg, regardless of modulation method. The auxiliary resonant snubber is combined with a new interleaved topology developed for the little box challenge and switching frequency is pushed to hundreds of kilohertz.

The following sections will detail operation of the inverter, design tradeoffs and considerations, and experimental results from prototype testing.

## 2 Inverter Operation

An interleaved auxiliary resonant inverter is able to achieve significant advances in power density by pushing the switching frequency of wide-bandgap devices, with the help of soft switching, to hundreds of kilohertz. The ZVS method could be appropriate for a range of inverter power levels, but when combined with interleaving can be efficiently used for inverters in the 2kW-6.6kW range.

Hard switching operation of the interleaved inverter with unipolar switching was discussed in section 1.2. The two high frequency legs, shown as Q1-Q4 in Figure 12, achieve ZVS by adding the auxiliary components discussed in section 1.3. The low frequency leg switches at 60Hz where switching losses are significantly smaller than conduction losses and the additional hardware for ZVS is not as beneficial. The final proposed topology is presented in Figure 12.

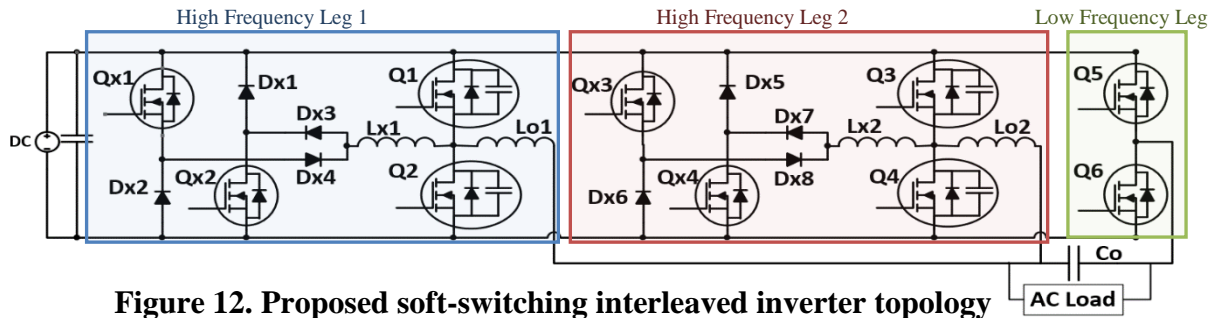


**Figure 12. Proposed soft-switching interleaved inverter topology**

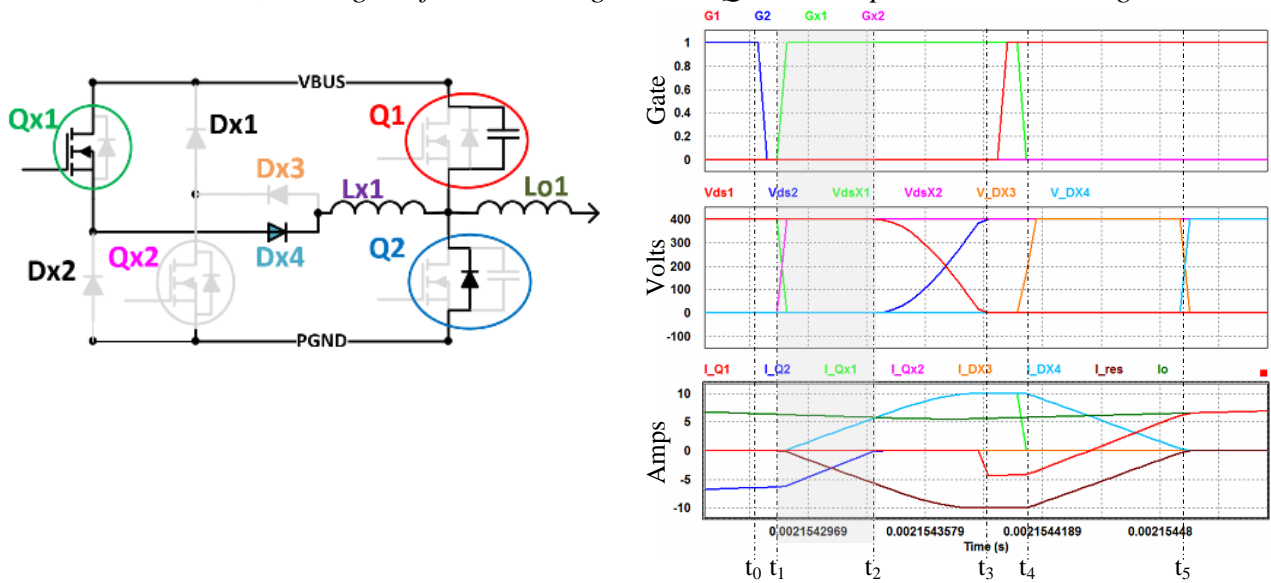
$L_{x1}$  and  $L_{x2}$  are auxiliary inductors that resonate with the drain-source capacitance of the main switches. The main MOSFET switches are  $Q_1$  and  $Q_2$  for leg 1 and  $Q_3$  and  $Q_4$  for leg 2.  $Q_{x1}$ ,  $Q_{x2}$ ,  $Q_{x3}$ , and  $Q_{x4}$  are auxiliary MOSFETs and  $D_{x1}$ - $D_{x8}$  are auxiliary diodes that assist the main switches in achieving zero voltage switching (ZVS). These auxiliary devices also operate at zero current switching (ZCS).  $Q_5$  and  $Q_6$  are low frequency MOSFETs..

### 2.1 ZVS Operation

As discussed in section 1.2 and shown in Figure 6, the two high frequency legs,  $Q_1$ ,  $Q_2$  and  $Q_3$ ,  $Q_4$  share the same references but with carriers separated 180 degrees out of phase. The low

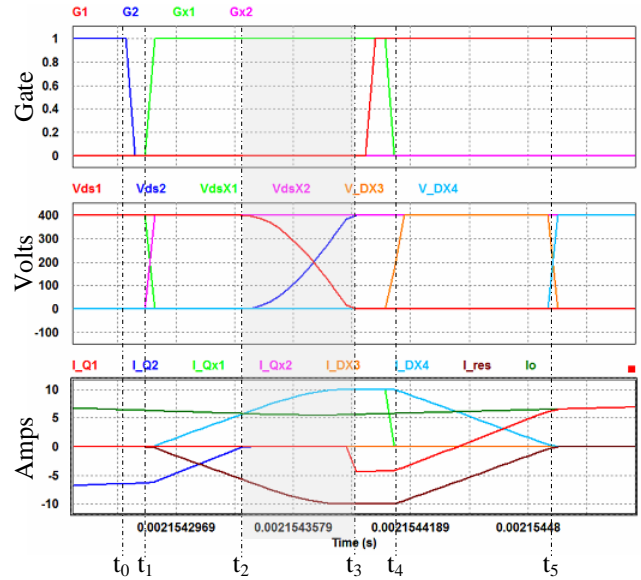
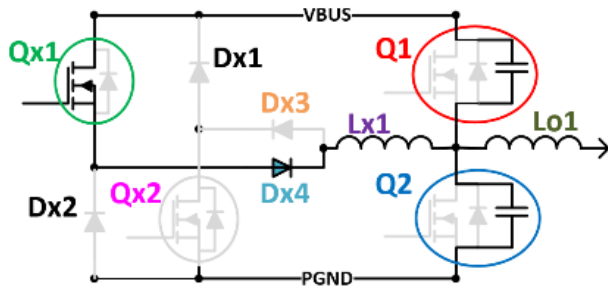
frequency leg switches at line frequency. The auxiliary components used to achieve ZVS operate only during dead time. Thus, on the larger 60Hz scale, the modulation waveforms of Figure 6 remain true, while on a smaller time scale the nanoseconds of deadtime between main switch turn-off and turn-on where ZVS is achieved is detailed below. The operation of the ZVS circuit is described in Figure 13. Here, five stages are shown between when the bottom switch Q2 is turned off, the auxiliary circuit is enabled, and the top switch Q1 is turned on under ZVS. The same procedure can be mirrored to achieve ZVS at turn-on of the bottom switch, Q2. Operation in the second, interleaved high frequency leg is the same. For clarity, the gate signal, voltage across, and current through each device are kept the same color as the diagram symbol e.g. all waveforms related to Q1 are red.

*[t<sub>0</sub>]: At t<sub>0</sub> the bottom switch Q2 turns off with zero voltage. The anti-parallel diode of Q2 temporarily conducts the current, leaving the full bus voltage across Q1 with output current unchanged*



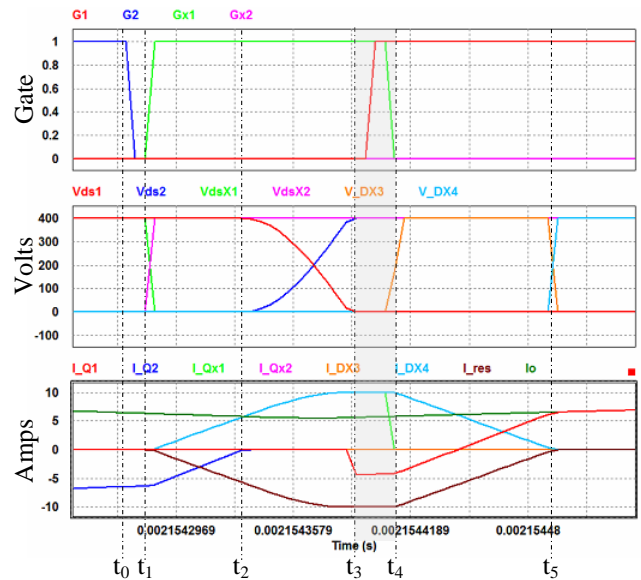
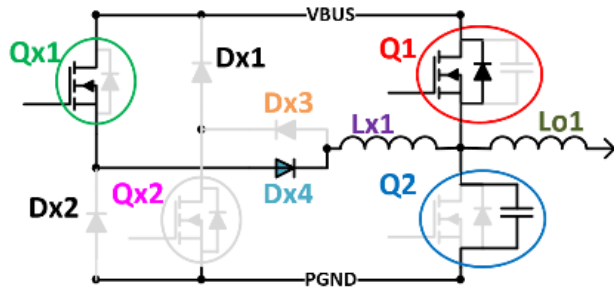
(a) Operation between [t<sub>1</sub>,t<sub>2</sub>]

*[t<sub>1</sub>-t<sub>2</sub>]: At t<sub>1</sub> the auxiliary switch Q<sub>x1</sub> turns on and current begins to flow through Q<sub>x1</sub> and D<sub>x4</sub>, linearly increasing auxiliary current as L<sub>x1</sub> charges. Simultaneously the current through Q<sub>2</sub>'s anti-parallel diode decreases linearly as the auxiliary current takes over providing the output current to L<sub>1</sub>.*



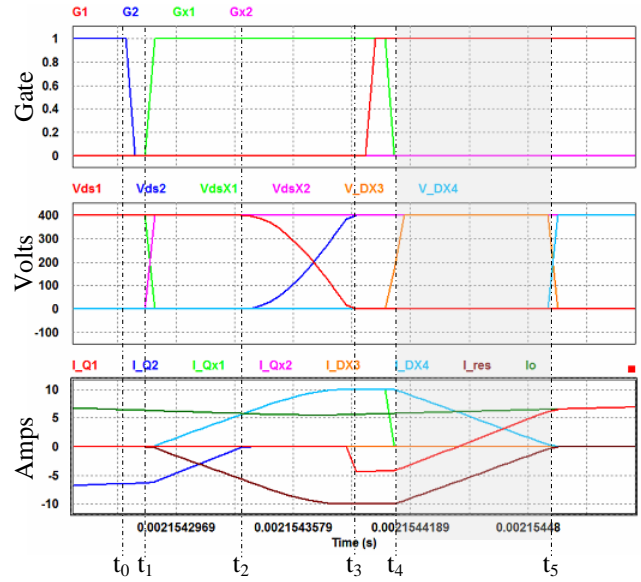
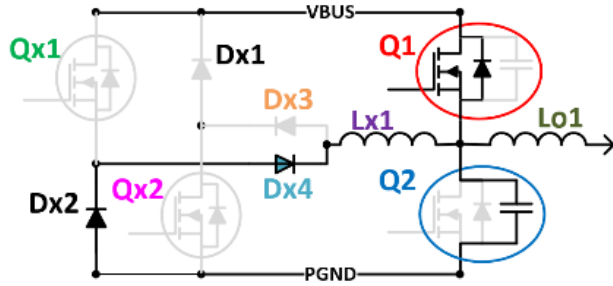
(b) Operation between  $[t_2, t_3]$

$[t_2-t_3]$ : At  $t_2$  the auxiliary current matches the output current and  $Q_2$ 's anti-parallel diode no longer conducts any current. Now, a sinusoidal resonance current forms between the auxiliary inductor  $L_{x1}$  and the drain-source capacitance of the main switches  $Q_1$  and  $Q_2$ . The resonance current exceeds the output current to discharge  $Q_1$  capacitor voltage and charge  $Q_2$  capacitor voltage to the bus voltage. No current flows through  $D_{x3}$  as the voltage across both  $D_{x2}$  and  $Q_{x2}$  is the bus voltage.



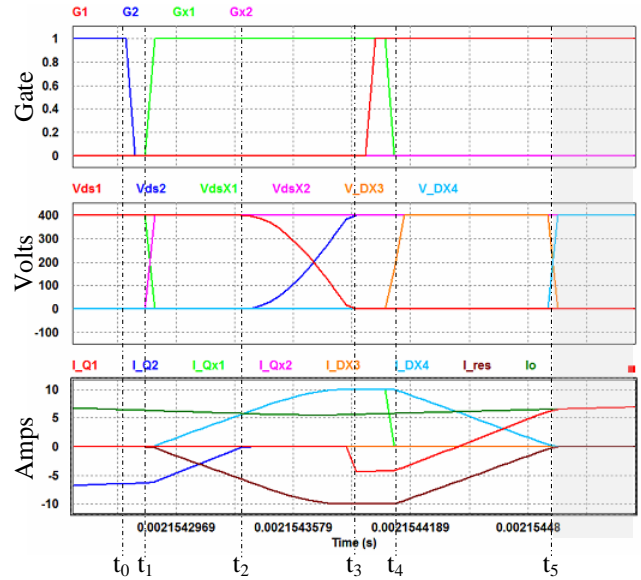
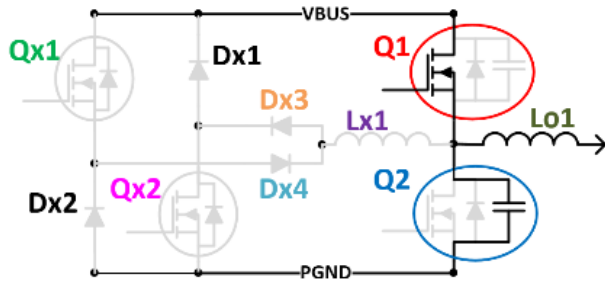
(c) Operation between  $[t_3, t_4]$

$[t_3-t_4]$ : Between  $t_3$  and  $t_4$   $Q_1$  voltage is completely drained and the MOSFET is turned on under zero voltage. The excess auxiliary resonant current momentarily travels through  $Q_1$ 's anti-parallel diode before turn-on and then through the channel after turn-on.



(d) Operation between  $[t_4, t_5]$

$[t_4-t_5]$ : At  $t_4$  the auxiliary switch turns off,  $D_{x2}$  begins to conduct, and the resonant current decreases non-linearly until it is equal to the output current. Then, auxiliary current decreases linearly to zero while the current through  $Q_1$  becomes positive and increases linearly.



(e) Operation from  $t_5$  until the next switching period

*[ $t_5$ ]: At  $t_5$  the auxiliary current reaches zero,  $D_{x4}$  begins blocking voltage and none of the auxiliary components are conducting current or turned on. The full output current for this leg is now handled by  $Q_1$  for the remainder of the switching period.*

**Figure 13. Topological and timing circuit operation.**

(For clarity, the gate signal, voltage across, and current through each device are kept the same color as the diagram symbol e.g. all waveforms related to  $Q_1$  are red.)

When output current is large enough, the bottom switch (when output current is positive) and the top switch (when output current is negative) can naturally achieve ZVS during dead time without the assistance of the auxiliary switches. This is because the output current can naturally drain away the voltage across the main switch drain-source capacitor. To further improve efficiency, auxiliary switching can be turned off for a switch while it naturally achieves ZVS, reducing switching loss. This is summarized in Figure 14.

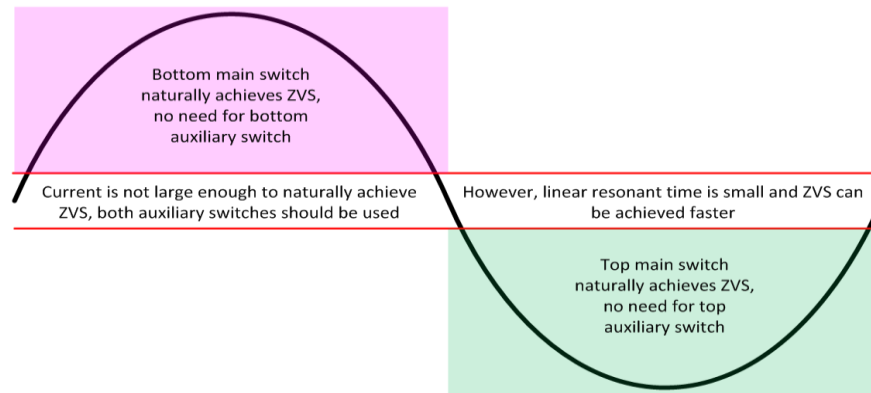


**Figure 14 Output current direction and magnitude impact on natural ZVS**

### 3 Design Tradeoffs and Prototype Hardware Selection

---

To verify the workings of this topology and prove that significant gains in power density can be made, a prototype was designed, built, and tested. The most common on-board electric vehicle charger is rated for 6.6kW so this was the power level chosen for the prototype. The prototype specifications are summarized in Table 2. While this stage would normally operate as a rectifier for EV charging, this topology will eventually be implemented with bi-directional capabilities and implementing it here as an inverter will allow for a simpler comparison with the hard-switching inverter developed for Google’s Little Box Challenge.

**Table 2. Prototype Specifications**

Parameter	Value
Input Voltage	400V
Output Voltage	220Vac
Power Level	6.6kW

#### 3.1 Dead Time and the Resonant Circuit

A linear period and a resonant period of time are required for the auxiliary current to assist the main switch in achieving ZVS. The linear period,  $[t_1-t_2]$  in Figure 13, occurs as the inductor current charges linearly to the load current level. This timing is dependent on the bus voltage, auxiliary inductance, and load current, and is obtained by:

$$V_{L_{x1}} = L_{x1} \frac{\Delta i_{aux}}{\Delta t} \quad (1)$$

$$V_{bus} = L_{x1} \frac{I_{load}}{t_{linear}} \quad (2)$$

$$t_{linear} = \frac{L_{x1} I_{load}}{V_{bus}} \quad (3)$$

The resonant period is defined as when auxiliary current surpasses output current at  $t_2$  and auxiliary current drops back below output current between  $t_4$  and  $t_5$  in Figure 13. The equivalent resonant circuit during this time is shown in Figure 15.

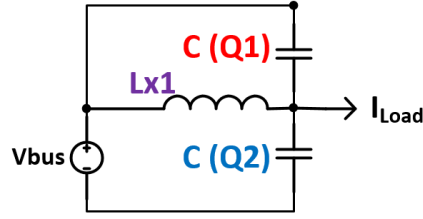


**Figure 15. Equivalent circuit during resonant period**

The time period  $[t_2-t_3]$  to reach ZVS can be described as:

$$t_{ZVS} = \frac{\pi}{\omega_{res}} \quad (4)$$

where

$$\omega_{res} = \frac{1}{\sqrt{L_{res}C_{res}}} = \frac{1}{\sqrt{L_{x1}(C_{Q1} + C_{Q2})}} \quad (5)$$

Thus, the amount of dead time required to achieve ZVS is summarized as:

$$\begin{aligned} t_{dead\ time} &= t_{linear} + t_{ZVS} \\ &= \frac{L_{x1}I_{load}}{V_{bus}} + \pi\sqrt{L_{x1}(C_{Q1} + C_{Q2})} \quad (6) \end{aligned}$$

Based on Equation (6), the linear period of dead time increases with load while the resonant period of dead time to achieve ZVS is constant regardless of load. By monitoring the output current for high frequency legs 1 and 2, dead time can be adjusted to accommodate changes in load, maintaining soft-switching from light load to full load. A minimum dead time is set based on the required resonant time,  $t_{ZVS}$ , which can be measured and calibrated on a prototype for guaranteed ZVS. Then, the linear dead time required can be updated with each current sensor sample to allow the system to easily adapt to different load conditions while minimizing dead-time related losses. As shown in Figure 6 (b), the peak duty cycle value occurs when output current is largest while the minimum duty cycle value occurs when the output current is smallest. Thus, adapting to changing levels of output current minimizes the impact of dead time on duty cycle as well: when output current is large, the duty cycle is longer and better able to handle the extra dead time required for ZVS; when output current is small, dead time can be scaled back to the minimum and consume less of the small on-time of the switch.

In actuality, with the implementation of adaptive dead time, loss of ZVS is less related to load current; instead, as switching frequency is pushed higher, dead time needs to be controlled to a small percentage of the switching period. Although, ZVS may be given up near the minimum duty cycle where on-time of the switch could be smaller than the necessary dead time.

### 3.2 Resonant Component Design Tradeoffs

As demonstrated in Equation (6), when resonant capacitance is increased,  $t_{ZVS}$  increases. When auxiliary inductance increases both  $t_{linear}$  and  $t_{ZVS}$  are increased. For this prototype, the natural drain-source capacitance of the transistor served as the resonant capacitance. One of the advantages of GaN is the small drain-source capacitance because of the reduction in package size, allowing it to achieve higher switching frequencies. Preserving this feature was an important design consideration. However, the non-linearity of the drain-source capacitance across changes in voltage can impact the predictability of dead time. Adding an additional external capacitor could provide a more constant source of capacitance while decreasing device turn-off loss. Yet, this must be weighed against an increase in dead time requirements.

Design of the resonant inductor must also consider several tradeoffs including dead time length and resonant current peak. Dead time length should be kept below about 5% of the switching period to minimize the impact of dead time on the output. With a larger resonant inductor, resonant time increases, creating more conduction loss in the resonant circuit. Vice versa, when resonant inductance is too small, the resonant current can spike up to higher current levels to reach ZVS, placing stress on the auxiliary devices. Thus, the largest inductance that still meets dead time requirements should be chosen.

For example, if 400kHz switching frequency is selected, the dead time should be kept under 5% of 2.5us or 125ns. To make calculations simpler a constant drain-source capacitance of 130pF is used. A 400V DC bus and 30A (15A per high frequency leg) output is used based on a 6.6kW inverter with 220V AC output. Furthermore, because adaptive dead time will assist the circuit in reaching ZVS at larger load currents, only half of the maximum load current for one high frequency leg is considered here.

$$t_{dead\ time} \geq \frac{1}{2} * \frac{L_{x1} I_{load}}{V_{bus}} + \pi \sqrt{L_{x1} (C_{Q1} + C_{Q2})} \quad (7)$$

$$125ns \geq \frac{1}{2} * \frac{L_{x1} 15A}{400V} + \pi \sqrt{L_{x1} (260pF)} \quad (8)$$

With these considerations, a 2.5uH auxiliary inductor is suitable, though further refinement through prototyping is necessary for confirmation.

At such small resonant values, material constraints can also come into play. The resonant frequency can be defined as  $\omega_{res}/2\pi$  (as in equation 5). Continuing with the above example, if resonant capacitance is 130pF and resonant inductance is 2.5uH, the resonant frequency is approximately 8.8MHz. To be fair, the true resonant current frequency could be less than that as the current will experience both linear and resonant time periods during dead time. Yet, this frequency range still proved difficult to find suitable ferrite cores. A summary of potential materials is listed in Table 3.

**Table 3. Core Material Options for Resonant Inductor**

Name	Manufacturer	Ferrite Type	Max Frequency
3F5	FerroxCube	MnZn	5MHz
P61	Acme	MnZn	6MHz
4F1	FerroxCube	NiZn	10MHz

In addition, many litz wire distributors will only rate their thinnest wire “up to 2MHz”, implying that these inductors will suffer from skin-effect related conduction losses or require more precisely-designed PCB windings. Of course, many more factors enter into magnetics design, but material limitations should be considered when weighing design tradeoffs.

For this prototype, P61 RM6 core samples were obtained and the resonant inductance was boosted slightly to try to remain within the 6MHz cutoff.

### 3.3 Switching frequency

Switching frequency is one of the most important factors in pushing power density. Soft-switching and GaN devices are implemented to push switching frequency while minimizing losses. While the auxiliary snubber will increase the PCB size with additional active components, passive components can be shrunk significantly to decrease the overall size.

Yet, dead time requirements and switching losses must be considered as well. Table 4 below provides a snapshot of these tradeoffs: as switching frequency is increased, the required filter inductance decreases but so does the available dead time for ZVS. For simpler comparison, the

table assumes that dead time constitutes 5% of the switching period and that the output filter capacitance is 1uF with a cutoff frequency one decade below the switching frequency. Of course, many other parameters are influential in a final design.

**Table 4 Switching frequency design tradeoffs**

Switching Frequency	Available Dead Time	Output Filter Inductance
200kHz	250ns	63.3uH
300kHz	166ns	28.1uH
400kHz	125ns	15.8uH
500kHz	100ns	10uH

For this prototype, 300kHz is selected for testing and verification of design. With further thermal handling and efficiency optimization, this design could be pushed further to between 400kHz – 500kHz for higher power densities.

### 3.4 DC Bus Voltage

While the specifications in Table 2 list a 400V DC bus, the final implementation of the inverter will include a dc/dc stage to interface with the electric vehicle batteries, provide double line ripple rejection, and boost/buck the voltage for the dc/ac stage if necessary. Keeping the voltage lower can allow the modulation index to be higher, allowing for optimal efficiency. Furthermore, a lower voltage permits the use of smaller 400V or 450V rated capacitors for the bus. However, it should be noted that the linear period of resonant current during dead time may take longer due to the decrease in available forcing voltage. Equations 9 and 10 below show the modulation index calculation.

$$D_{max} = 1 - t_{dead\ time} * f_s \quad (9)$$

$$\frac{v_o}{v_{dc}} = M = 2D_{max} - 1 \quad (10)$$

With a rounded-up dead time of 170ns, a switching frequency of 300kHz, and an output voltage of 220Vrms (311Vpk), the bus voltage must be larger than 345V. For additional margin, testing is performed between 350V-360Vdc.

### 3.5 Auxiliary Active Component Selection

The auxiliary switch is chosen to meet voltage, current, and switching requirements. While the auxiliary switch should face fewer stresses than a main switch, the two must operate at the same high frequency, which ultimately proves to be the largest constraint on device selection. If the input is a maximum of 400V, with lifetime and safety de-ratings, a transistor with at least 600V blocking capability should be selected.

Across the switching period, the resonant current (and thus the current through the auxiliary switch) spikes to just above the load current level during dead time and then remains off for the rest of the period. This produces a relatively large peak current but an overall small rms current, as shown in Figure 16. This makes selecting a transistor with the proper current rating somewhat challenging as most specify a maximum continuous current while being able to handle significantly larger pulse currents. Furthermore, because the auxiliary rms current is low, the on-state resistance of the device selected is not a driving factor for selection.

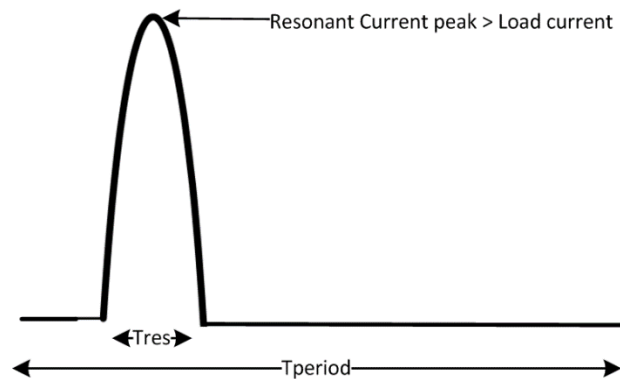


**Figure 16 Resonant Current over high frequency leg switching period**

Ultimately, turn-on and turn-off of the transistor was one of the most important elements in ensuring the device could turn on and off quickly within the small dead time window. This factor alone eliminated the option of IGBTs. While Si-MOSFETs have significantly faster turn-on/off times, many still consume tens of nanoseconds. Switching losses will also be the majority of losses for these auxiliary devices and  $C_{oss}$ ,  $E_{on}/E_{off}$  should be considered.

GaN System's GS66508P is chosen as the auxiliary switch. It is rated for 650V<sub>DS</sub>, 30A continuous current, 50mΩ drain-source on resistance, and rise and fall times of under 6ns. For cost savings, a silicon MOSFET could also be used here.

Auxiliary diodes must conform to the same criteria as the auxiliary switch in terms of blocking voltage and current handling. Like GaN, SiC offers zero reverse recovery, minimizing switching loss. The Cree Sic C3D1P7060Q 600V, 1.7A rated Schottky diode is selected for all four auxiliary diodes. Again, though the stated current rating is small, the diode also specifies that its peak forward current pulse rating is 40A for 10us – both this current and time duration are larger than our application will require. This diode also has an attractive small QFN package size, minimizing parasitic capacitance and reducing the impact of additional auxiliary components on PCB size.

### **3.6 Main Switch Selection for High Frequency Legs**

The main switch is chosen to meet voltage, current, and switching requirements of the interleaved inverter high frequency legs. These switches must handle the main power of the inverter. At 6.6kW and 220Vac output, the total output rms current will be 30A. Ideally, this current is shared by the two interleaved legs so each transistor must handle 15Arms. A small on-state resistance will help reduce conduction loss. The minimum voltage rating of the device should be 600V.

While previously there were very few high-voltage GaN devices available with many proving unreliable or hard to work with, the technology is beginning to mature and more devices with more voltages from more companies are beginning to emerge. In 2014, GaN Systems became the first company to release a 650V rated GaN enhancement mode transistor. Their unique method of manufacturing significantly reduced parasitic inductance for reduced noise when switching. This project chose GS66516T 650V, 60A, 25mΩ E-mode transistor. This same device was chosen for FEEC's entry into the Little Box Challenge and survived 100 hours of testing for both our team and the first place finisher's.

Importantly, this device's thermal pad is on the top of the package. Because the package is so thin, all main switches can be attached to the bottom of the PCB and directly connected to a larger heat sink while gating and other components populate the top of the PCB. At the peak power of 6.6kW, each transistor must dissipate 5.6W of loss, which may prove difficult for such a small package. Direct heat-sinking to spread the heat will be crucial.

### 3.7 Challenges in Driving GaN

One challenge in using GaN was design of the gate-driving circuit. Fast switching transition noise coupled with parasitics can interfere with the control circuit, at time falsely turning on or off the transistor. To combat this in FEEC's entry to the Little Box Challenge, a Silicon Lab Si8261BAC driver and a custom-designed 12V to 7V isolated power supply was used for each device. An opto-coupler based gated driver is good for common mode noise immunity, but it occupies a lot of space and introduces propagation delay. The Silicon Lab gate driver chip instead employs an LED emulator that mimics the operation of a traditional optocoupler but within a smaller volume and with shorter delays.

Yet, even with these features, it was found that the false turn-on/off persisted. Thus, a new configuration is set up between the PWM signal of the dsp and the input to the gate driver chip. This operation is shown in Figure 17 and Figure 18 and is originally described by the creator in [8].

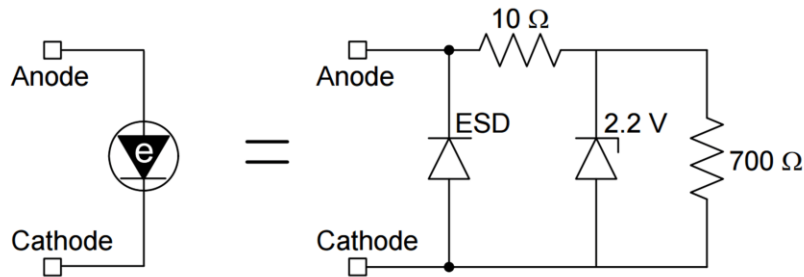


**Figure 17. Equivalent electrical configuration of Silicon Labs gate driver signal input**

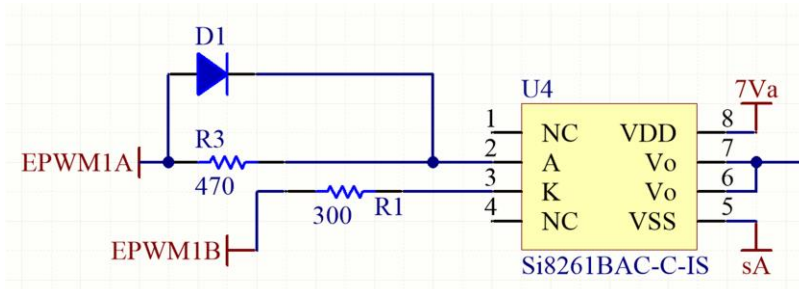


**Figure 18. Layout for added reliability of gate drive circuit**

The DSP PWM signals A and B are used to drive a half-bridge with complementary switching. Thus, when gate signal A is high, B must be low and vice versa. Thus, in Figure 18, when the EPWM1A signal is high, the EPWM1B signal must be low and the gate driver U4 is enabled with positive voltage. When EPWM1B is high and EPWM1A is low, U4 is disabled

with negative voltage and the reverse diode of U4, shown in Figure 17, conducts the reverse current. The output pins  $V_o$  on U4 then connect to turn-on/off resistors and then to G1. While two PWM signals are input into the circuit for error reduction, only one transistor is driven with each gate drive circuit. Compared to the original design where K is connected to ground, this method has proven to be more reliable.

Figure 19 shows the gating and transistor layout on the PCB for the Little Box Challenge. To minimize noise and parasitics, top and bottom switches within a half-bridge leg should be placed as close together as possible. The gate drive signal should also be placed as close to the gate as possible, with any potential ground loops shrunk in length.

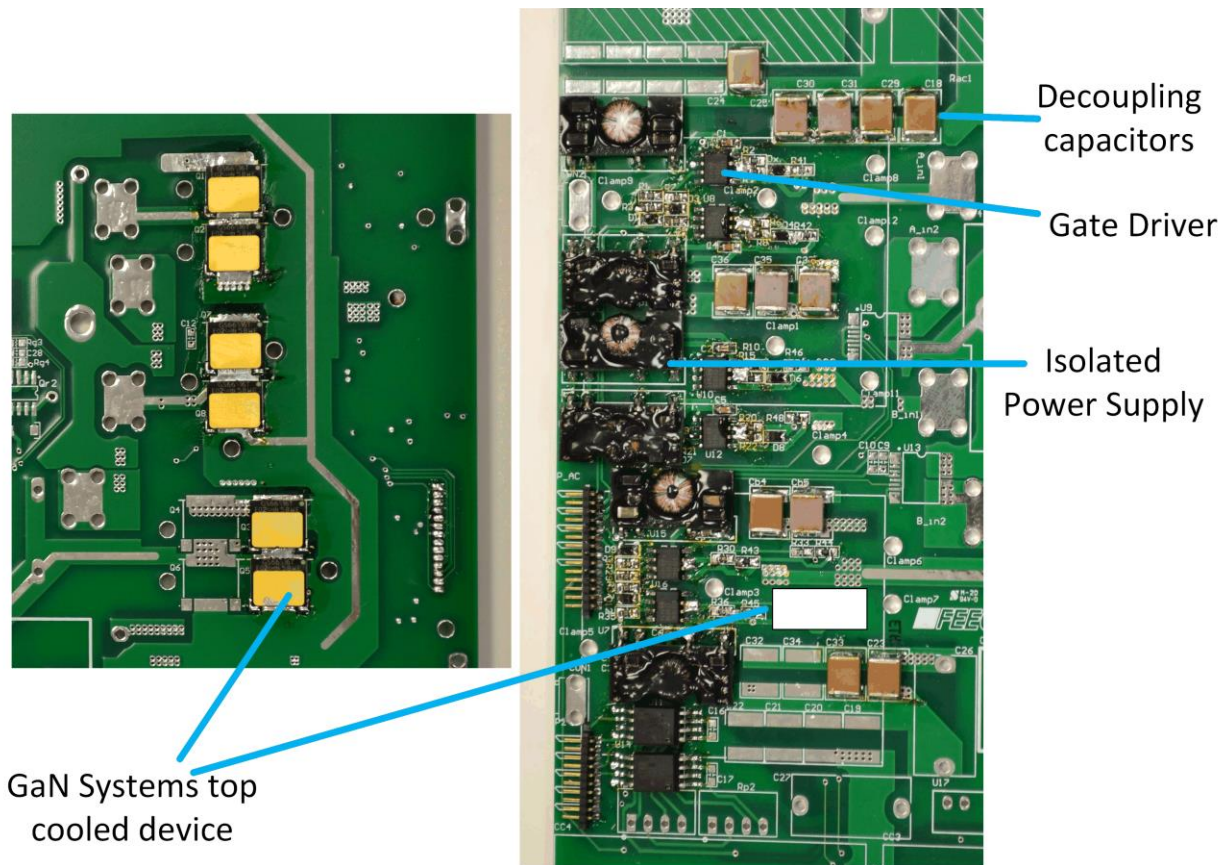


**Figure 19 Gating and Switch layout for Little Box Challenge PCB**

The GaN Systems device requires a gate voltage of between 6.5V-7V, which proves complicated to achieve as traditional gate power supplies are not available at that voltage, not isolated, or not precise enough. Too small a gate voltage and the transistor is not fully turned on;

too large a gate voltage and the transistor can fail. For the little box challenge, custom isolated 12V to 7V power supplies were created (shown in Figure 19) that provided power for each transistor.

For the eight GaN transistors used in the two high frequency legs for the soft-switching topology introduced in section 2, the volume of eight isolated power supplies began to become too large. A solution was found in a newly released GaN Systems evaluation board's schematic, shown in Figure 20. A bootstrap gate driver is a common solution for a high-side switch where the source pin is not connected to ground and a floating ground must be used for the associated power supply and gate driver. When the bottom transistor is on, the source pin of the top switch is pulled to ground and a capacitor is charged to the gate voltage. When the bottom transistor is turned off and the top switch is signaled to turn on, the capacitor discharges to provide a voltage to the gate driver while a diode blocks any current from flowing back to the charging source. Because of the variable nature of a voltage source being a discharging capacitor, this option would normally not be precise enough to reliably drive a GaN switch. Cleverly, the evaluation board solves this issue by bootstrapping a small IC buck converter with internal comparator to reliably supply the desired gate voltage despite fluctuations in the input voltage.

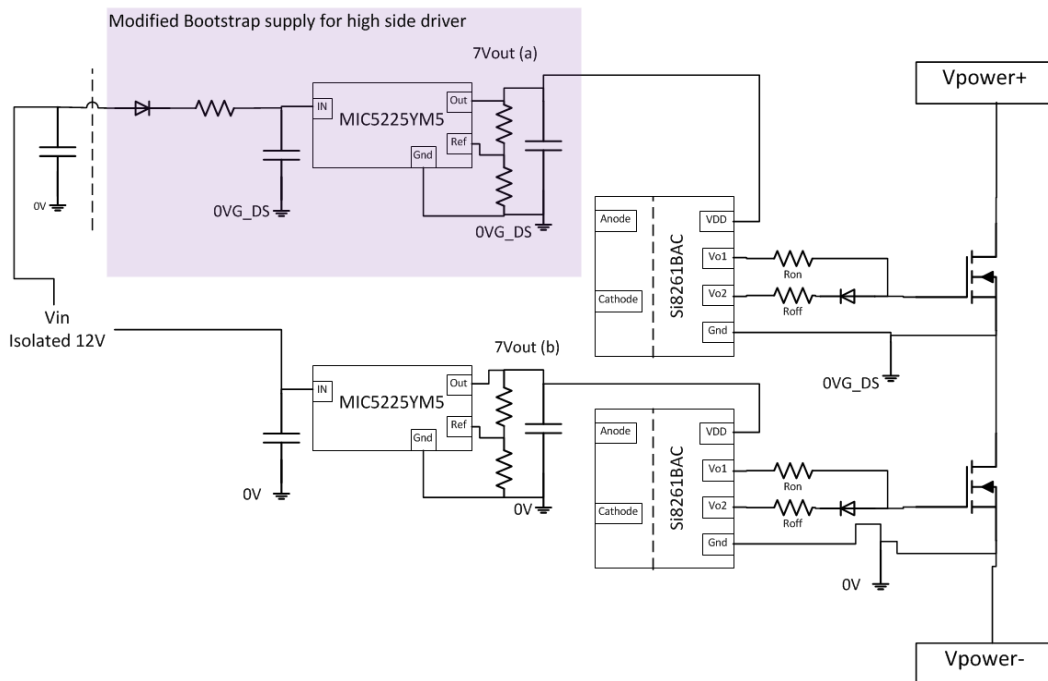


**Figure 20. Modified bootstrap circuit for GaN transistor gate voltage supply**

The designed prototype combines these two approaches by using an isolated power supply for each leg of the inverter and a modified bootstrap circuit for the high-side switches within that leg. This method has proven to be just as reliable while consuming less space. The modified bootstrap method also allows for a greater level of control and freedom when selecting a precise gate drive voltage. This allows the designer to both better protect the GaN transistor while ensuring full turn-on.

### **3.8 Main Switch Selection for Low Frequency Leg**

The low frequency leg is much more simplistic in design. At 60Hz, switching losses are minimal. However, this leg must bear the full power current load of 30A. Infineon's IPW65R019C7 is selected for its low on-state resistance of 17m $\Omega$ . This silicon MOSFET is rated for 650V and 75A. Yet at full power, a single TO-247 switch would have to dissipate at least 15W of loss. To assist with thermal handling and improve efficiency, two Infineon MOSFETs are placed in parallel to cut the conduction loss in half. To further aid in thermal dissipation, the four MOSFETs are hung off the edge of the PC board and directly attached to the same heatsink as the main switches on the high frequency leg.

### **3.9 Output Filter**

The output inductor-capacitor low pass filter takes in the unipolar square wave, filters out the switching frequency and its harmonics, and outputs a smooth AC waveform. As in Table 4, the corner frequency of the filter can be first designed as one decade below the switching frequency. At heart, greater power density comes from pushing this corner frequency to higher frequencies and reducing the size of the filter. Using GaN, implementing ZVS, and pushing the switching frequency to hundreds of kHz was all implemented in an effort to shrink the volume of bulky passive components.

Equation 11 below summarizes the relationship between the output filter values and the cutoff frequency. For the capacitance, surface mount ceramic or film capacitors are preferred over bulkier or less reliable other materials. For now, 1 $\mu$ F is chosen as either a standard value of film capacitor could be used or ten 0.1 $\mu$ F 650 COG could be placed in parallel on the PCB.

While film capacitors are attractive because of their reliability and the safeguard of their fail as open circuit, ceramic capacitors are smaller in size and can be easily surface mounted to the PCB.

$$f_c = \frac{1}{2\pi\sqrt{L_o C_o}} \quad (11)$$

Thus, assuming a corner frequency of one decade below the switching frequency, the output filter inductor should be 28.1uF. Each output inductor of the two high frequency legs would need to be this inductance. In testing, this value can be further refined. For example, having a larger current ripple could reduce zvs time as the auxiliary current would not have to charge to as high of a load current. Harmonic noise requirements and efficiency should also be considered. Unipolar modulation and interleaving should reduce filtering requirements.

## 4 Design Summary

A prototype was constructed to verify the design. The input bus voltage is 350V DC and 400/450V DC electrolytic capacitors are used in lieu of the dc/dc stage for double-line ripple suppression. The inverter is designed for 6.6kW with 220V AC output with a switching frequency of 300kHz.

**Table 5. Summary of prototype design**

Power level	6.6kW
Input DC Voltage	350V
Output AC Voltage	220V
Switching Frequency	300kHz
Main High Frequency switch	650V GaN MOSFET
Auxiliary switch	650V GaN MOSFET
Auxiliary Diode	1.7A SiC Schottky
Low Frequency Leg switch	650V Si MOSFET
Auxiliary inductor	3uH in P61 RM6 core
Output inductor	24uH in 3F3 RM12 core

### 4.1 Hardware Test Setup

With the components of Table 5, a PCB is designed and built to test the interleaved auxiliary resonant inverter. The PCB comprised of four layers of three-ounce copper for better current handling capability. Only the main GaN switches were mounted to the bottom of the PCB while the remaining components were mounted to the top of the PCB. Power components maintained a clear gap between the low voltage gating. High current areas were given large traces interlaced with one another such that most high power areas run in parallel across three or all of the four layers. To reduce parasitic inductance, high and low side switches were placed close to one another. The PCB design and populated board for testing are shown in Figure 21 and Figure 22, respectively. For sensor processing, fault detection, and gate control, a second in-house-designed board is attached to the main power PCB with a TI DSP TMS320F28069.

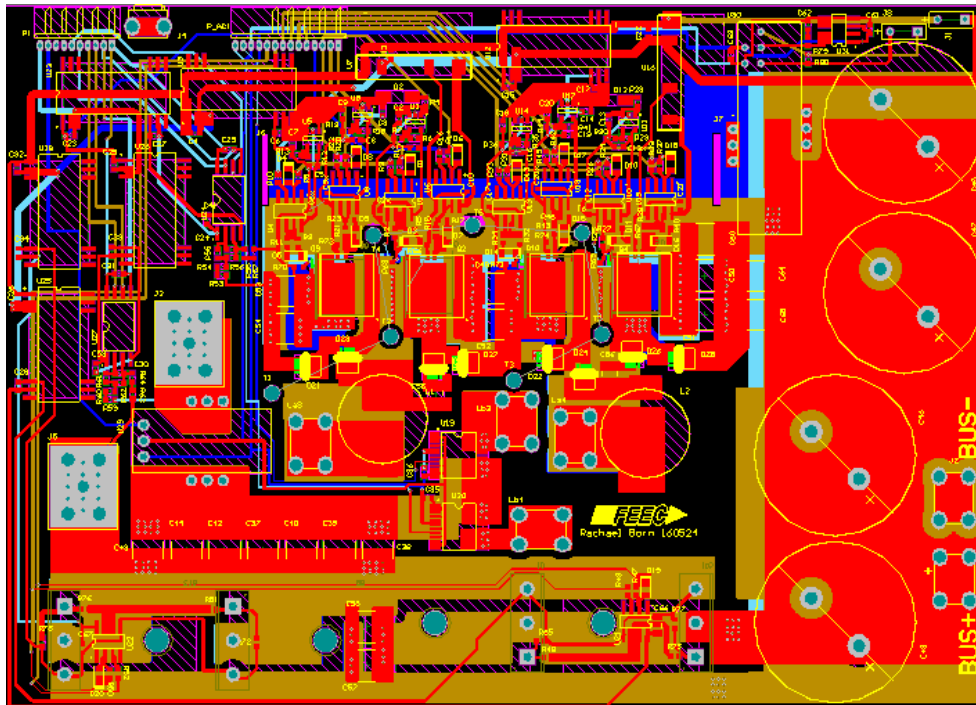


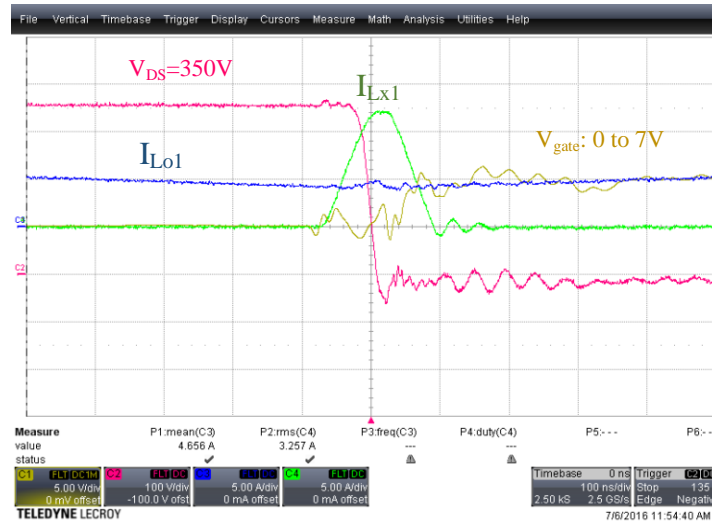
Figure 21 Altium PC Board layout



Figure 22. Assembled prototype for testing

## 4.2 Soft-switching

As shown in Figure 23, the red curve represents drain-source voltage starting at 350V before the auxiliary resonant current discharges  $V_{DS}$  to 0V. While there was some noise at the gate (yellow curve), possibly coupling noise from the probe itself, the gate does not turn on until after the voltage is drained, achieving ZVS. The resonant current begins at 0A and returns there shortly after the end of the dead time period, ensuring ZCS for the auxiliary switches.



**Figure 23. Auxiliary resonant circuit assists main switch to achieve ZVS**

This result confirms the operation principles of the auxiliary soft switching topology described in section 2 of this paper.

## 4.3 Power Density

Achieving soft switching required doubling the number of MOSFETs, adding several diodes, and two auxiliary inductors. Yet the extra diodes and transistors are active elements that are small and continue to decrease in size while increasing in functionality. Thus, power density relies on minimization of the output filter, keeping the auxiliary inductor small, form-factor awareness, and simplified thermal management.

Figure 22 shows the assembled prototype. The DSP PCB, current sensor, and input capacitors are all 1" tall. The resonant inductor is small enough to be directly anchored to the board. The output inductors will be placed on a platform sitting on top of the low profile areas of the PCB. The low frequency devices are hung over the side to provide easier access to the heat sink. The main high frequency switches are "top-cooled" and are attached to the bottom of the

PCB for easy heat sink mounting. The width of the unit from the edge of the DSP board to the low frequency MOSFETs is 5.5" and the length from the edge of the board to the over-hanging capacitors is 7.4".

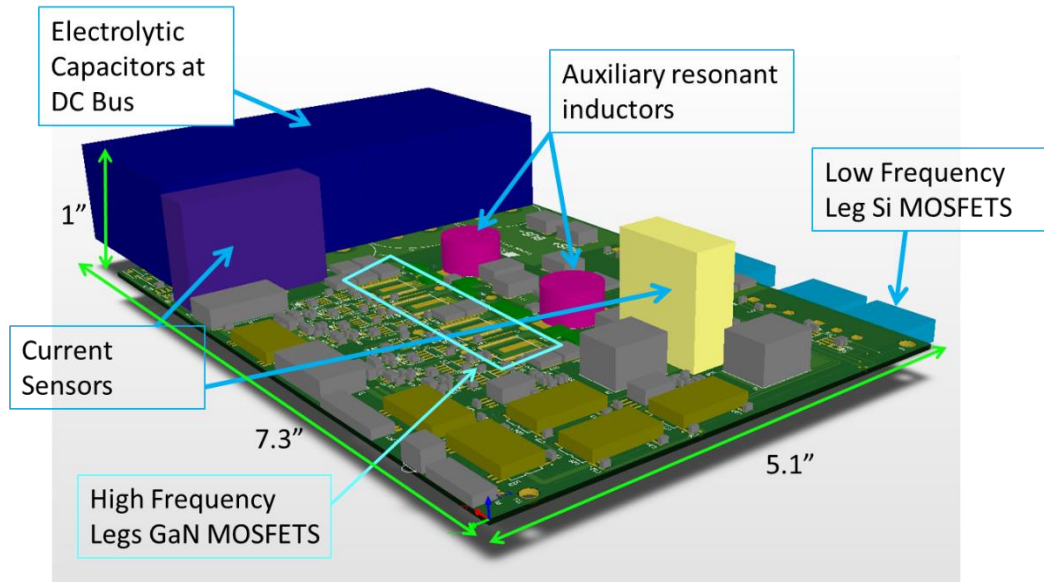


**Figure 24 Autocad model of soft-switching interleaved inverter**

This makes the predicted power density of the 6.6kW inverter to be  $160\text{W}/\text{in}^3$ . This number does not include heat sinking, an enclosure, or the eventual dc/dc stage (though presumably that stage would be the same size or smaller as the electrolytic capacitors which are included in this power density) and a final unit would have a smaller power density. For reference, Google's little box challenge required a power density of  $50\text{W}/\text{in}^3$  (system level) and the previous FEEC prototype was  $38.1\text{W}/\text{in}^3$  (system level).

While the soft-switching inverter must use twice as many components as the hard-switching version, PCB size was able to be well controlled to not increase too much in size. One space-saving strategy was to mount the main switch GaN on the bottom of the board and the auxiliary switch GaN directly overtop on the top of the board. Figure 25 shows a side by side comparison of a hard switching interleaved PCB and a soft-switching PCB. While the added components could mean an increase in cost, complexity this inverter has proven to be very promising in applications – such as electric vehicles and aerospace – where size and weight are major concerns.

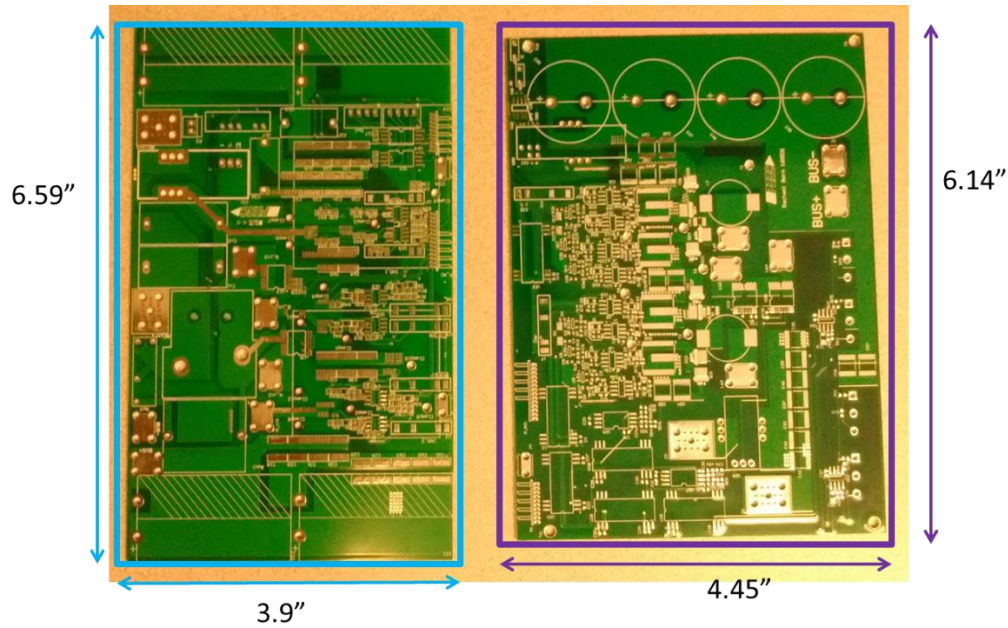


**Figure 25 PCB size for hard switching topology (left) and soft switching topology (right)**

#### **4.4 Zero Crossing Issue**

Unfortunately, an issue emerged that halted further power handling testing, efficiency examinations, and design parameter refinement. When the output AC waveforms crossed zero from either positive to negative or negative to positive, significant ringing occurs. This noise is short-lived but large – often larger than the output waveform itself. At even low power and voltage input, a protection circuit was consistently tripped, the zero crossing spike so significant the protection believed it was a shoot-through event. While perhaps the protection level could simply be boosted (it is already at twice the rated current), this could leave the sensitive (and pricey) GaN devices vulnerable while doing little to solve the real issue at hand.

First, ZVS and full-voltage handling capabilities were confirmed by keeping duty cycle constant and creating a DC output voltage instead of the desired AC waveform. The zero crossing spiking is also present in the hard switching interleaved inverter and does not seem to be impacted by the soft-switching circuit.

It must be noted that at the zero crossing, several drastic gating signal changes are made in one moment. A low frequency device turns off, followed by dead time and the other low frequency device turning on. The main switches of the interleaved high frequency legs change from the minimum duty cycle to a complementary signal at the largest duty cycle. This makes it

difficult to determine the origin of this spiking: unsynchronized switching, the change from low to high duty cycle and vice versa of the high frequency main switches, the drain-source capacitance of the low frequency leg resonating during dead time, or that with zero load current, spikes occur to quickly charge the low frequency leg drain-capacitance during turn-on.

First, the gate signals were fully synchronized at the zero crossing to test if this was the origin of the spiking. Synchronization requires more complex code because all of the main switching signals must be signaled to turn off together, despite differences in phase, remain off for the duration of the dead time, and then turn on together and return to their proper duty cycle and phase. The resulting synchronized gate signals are shown in Figure 26.

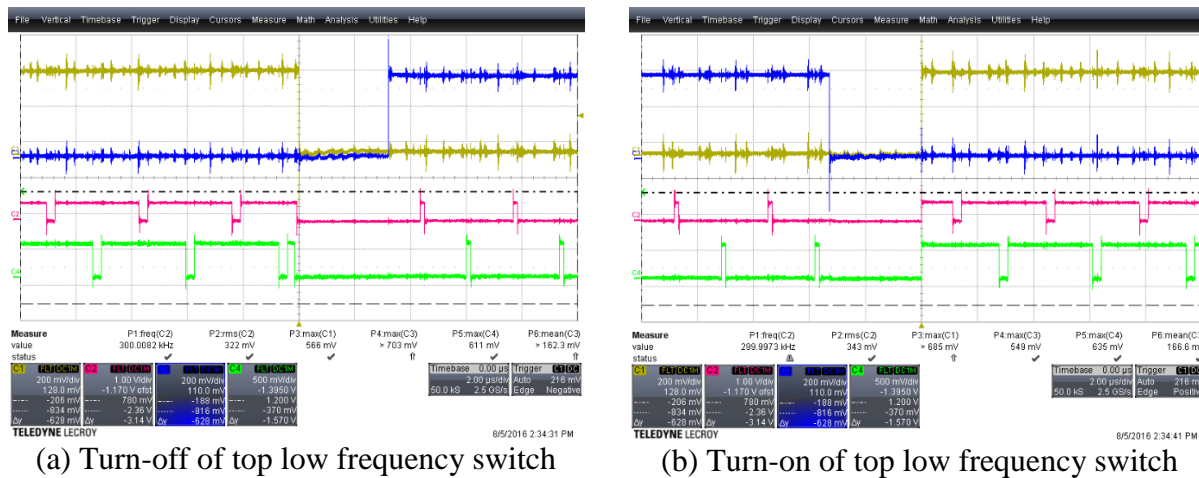


**Figure 26 Synchronized turn-on and turn-off of gate signals at zero crossing points.**

The yellow waveform is the top low frequency switch, blue is the bottom low frequency switch, red the top main switch of the first high frequency leg, and the green is the top main switch of the second high frequency leg

When compared with other strategies such as allowing the main switches to continue turning on/off during dead time, turning main switches on/off slightly before the low frequency's signal to turn on/off, etc, synchronizes switching showed the most improvement. Yet, the resonance remained, as shown in Figure 27. Though the image makes the noise appear somewhat small, the input voltage was only 10V and the input current spiked to more than double the peak of the rest of the waveform. As input voltage and output power increased, this relationship remained continued to harmful levels.

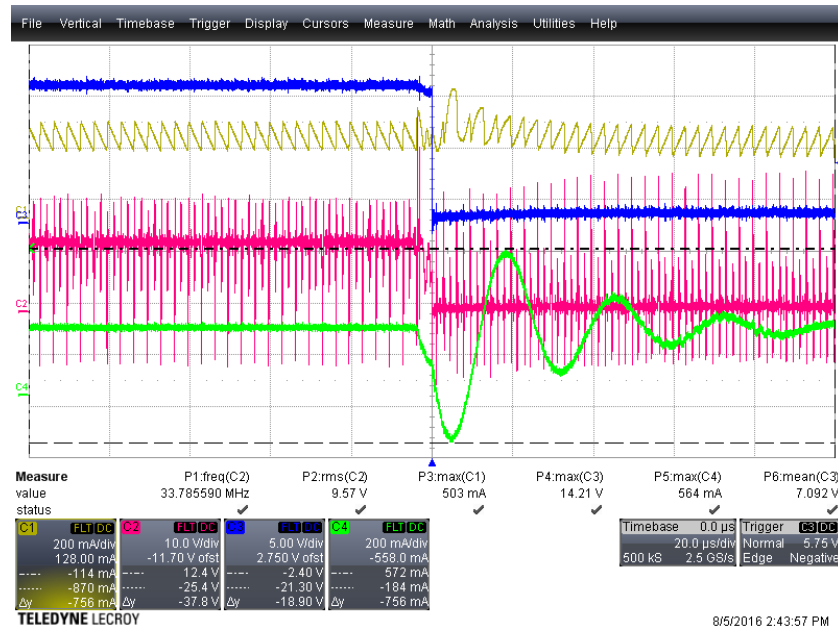


**Figure 27 Zero crossing waveforms as a result of synchronized turn-on/off.**

**The blue waveform represents the drain-source voltage of the top low frequency switch, red the drain-source voltage of the top switch of high frequency leg 1, yellow the output inductor current of high frequency leg 1, and green the input DC current.**

This spiking was never observed in the original PSIM simulations. After the zero crossing issue became pressing, non-ideal elements were added to the original ideal PSIM simulations and a small spike in current was observed at the zero crossing.

One method that completely eliminated noise in these simulation trials was turning off both all of the auxiliary switches and synchronous switching so that the inverter returned to the simpler modulation method introduced in Figure 4 in section 1.2 of this paper. To test this, the auxiliary and complementary switches were turned off 15us before the zero crossing and not turned on again until 15us afterward. The gating control waveforms are shown in Figure 28. Complementary switching is turned off just before the zero crossing so that only the main switch at minimum duty cycle is switched during the low frequency leg transition.

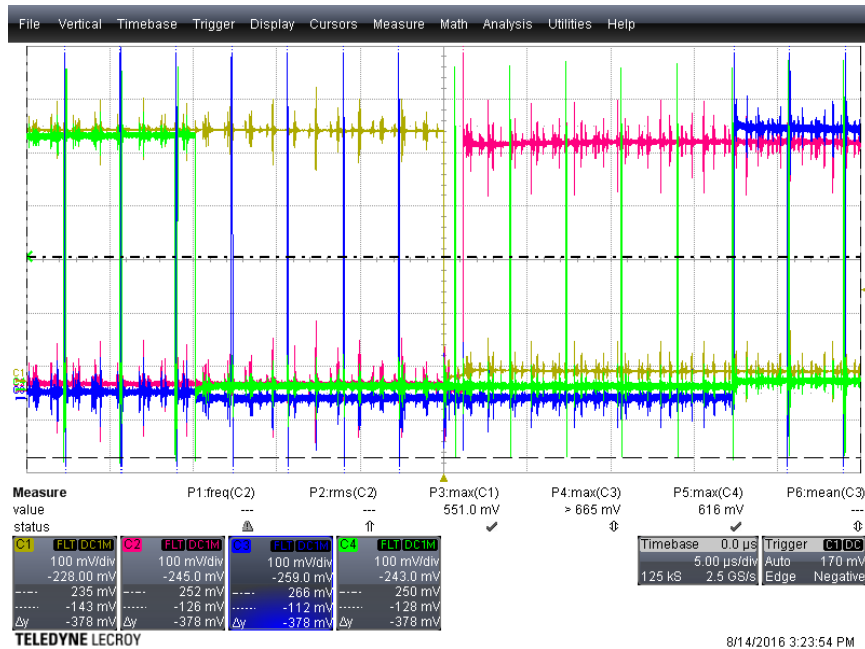


**Figure 28 Modified gating waveforms at zero crossing. The yellow and red waveforms control the low frequency legs and the green and blue waveforms control the main switches of a single high frequency leg.**

Unfortunately, while still smaller than other methods tried, the zero crossing issue remained at a level relatively unchanged from the previous configuration in Figure 27, as shown in Figure 29 and Figure 30.

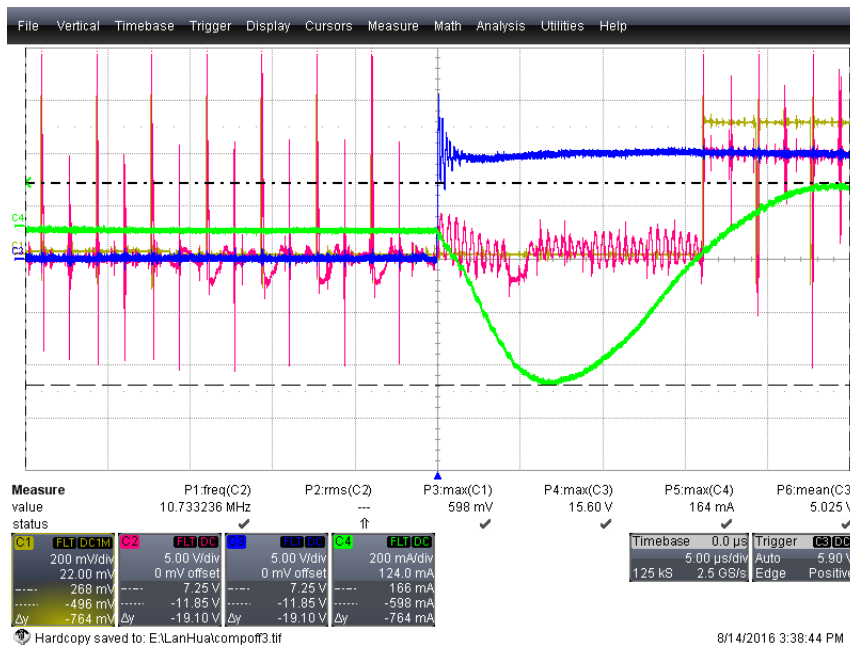


**Figure 29 Spikes in current remain despite the simplified gating around the zero crossing**



**Figure 30 Level of spiking on input and output current waveforms (bright and dark green, respectively) relative to level of current. The blue waveform is drain-source voltage of a low frequency switch and the red is the drain-source voltage of a high frequency switch.**

Thus, while changing the gating configurations was able to assist in the reduction of noise at the zero crossing, it could not eliminate it. Therefore, this issue is believed to not be related to synchronization or changes in duty cycle, but the transition from one low frequency device to another. As evidenced in both Figure 27 and Figure 29, the resonance begins at the voltage change of the low frequency leg device. While the gate signals provide plenty of dead time, the actual voltage transition between the two switches occurs when the first device is turned off and must charge to the full bus voltage. Yet at this moment is the zero crossing and there is very little current in the system to charge the switch. This leaves the circuit vulnerable to the observed resonance spikes.

## 5 Conclusion

---

The setback in managing the zero crossing must be further investigated and solved. While this paper focused on managing gate signal timing, perhaps other avenues of control such as hardware changes or closing the control loop may prove more fruitful.

If the zero crossing issue is solved, this topology shows incredible promise for pushing inverters to higher densities. Because several parameters could not be further refined through testing, several avenues of future work exist with this topology. Switching frequency can be pushed even further to 500kHz, though the impact on efficiency and available dead time should be closely monitored. Optimizing the auxiliary resonant inductor/capacitor relationship for achieving ZVS also requires further study. Finally, the combination of high switching frequency and soft-switching should minimize the necessary size of EMI filters, but must be tested and compared with the hard switching version.

A novel interleaved, soft-switching inverter is proposed. The mechanisms of interleaving are discussed as well as the decision making process for finding a soft-switching solution. The resonant circuit is analyzed to optimize the resonant components, find a suitable dead time length, and achieve ZVS across load conditions. Finally, a 6.6kW prototype was introduced that could reach 160W/in<sup>3</sup> power density.

## 6 Citations

---

- [1] Z. Liu, X. Huang, W. Zhang, F. C. Lee, and Q. Li, "Evaluation of high-voltage cascode GaN HEMT in different packages," in *2014 IEEE Applied Power Electronics Conference and Exposition - APEC 2014*, 2014, pp. 168-173.
- [2] T. Warren. (2016). *Tesla has received almost 400,000 preorders for the Model 3*.
- [3] B. Howard. (2016). *Model E: Now Ford plans a 200-mile electric vehicle*.
- [4] *Developing Infrastructure to Charge Plug-In Electric Vehicles*.
- [5] Z. Shahan. (2015). *Electric Car Charging 101 — Types of Charging, Charging Networks, Apps, & More!*
- [6] *Electric Vehicle Charging Infrastructure*.
- [7] *COOLER-SIZED ISN'T COOL*. Available: <https://www.littleboxchallenge.com/>
- [8] L. Zhang, R. Born, X. Zhao, and J. S. Lai, "A high efficiency inverter design for Google little box challenge," in *Wide Bandgap Power Devices and Applications (WiPDA), 2015 IEEE 3rd Workshop on*, 2015, pp. 319-322.
- [9] J. Dominic, "Comparison and Design of High Efficiency Microinverters for Photovoltaic Applications," M.S., Electrical and Computer Engineering, Virginia Tech, 2015.
- [10] D. M. Divan and G. Skibinski, "Zero-switching-loss inverters for high-power applications," *IEEE Transactions on Industry Applications*, vol. 25, pp. 634-643, 1989.
- [11] Q. Zhang, H. Hu, D. Zhang, X. Fang, Z. J. Shen, and I. Bartarseh, "A Controlled-Type ZVS Technique Without Auxiliary Components for the Low Power DC/AC Inverter," *IEEE Transactions on Power Electronics*, vol. 28, pp. 3287-3296, 2013.
- [12] W. Chien-Ming, "Nonlinear-controlled strategy for soft-switched series-resonant DC/AC inverter without auxiliary switches," *IEEE Transactions on Power Electronics*, vol. 18, pp. 764-774, 2003.
- [13] E. Faraci, "Design of a Resonant Snubber Inverter for Photovoltaic Inverter Systems," M.S., Electrical and Computer Engineering, Virginia Tech, 2014.
- [14] J. S. Lai, R. W. Young, D. Chen, M. B. Scudiere, G. W. Ott, C. P. White, *et al.*, "Resonant snubber inverter," ed: Google Patents, 1997.

- [15] J. S. Lai, R. W. Young, G. W. Ott, C. P. White, J. W. McKeever, and D. Chen, "A novel resonant snubber based soft-switching inverter," in *Applied Power Electronics Conference and Exposition, 1995. APEC '95. Conference Proceedings 1995., Tenth Annual, 1995*, pp. 797-803 vol.2.
- [16] I. Barbi and D. C. Martins, "A true PWM zero-voltage switching pole, with very low additional RMS current stress," in *Power Electronics Specialists Conference, 1991. PESC '91 Record., 22nd Annual IEEE, 1991*, pp. 261-267.
- [17] J. s. Lai, J. Zhang, H. Yu, and H. Kouns, "Source and Load Adaptive Design for a High-Power Soft-Switching Inverter," *IEEE Transactions on Power Electronics*, vol. 21, pp. 1667-1675, 2006.
- [18] K. M. Smith and K. M. Smedley, "A comparison of voltage-mode soft-switching methods for PWM converters," *IEEE Transactions on Power Electronics*, vol. 12, pp. 376-386, 1997.
- [19] Y. Xiaoming and I. Barbi, "Analysis, designing, and experimentation of a transformer-assisted PWM zero-voltage switching pole inverter," *IEEE Transactions on Power Electronics*, vol. 15, pp. 72-82, 2000.
- [20] B. Chen, J. S. Lai, C. L. Chen, W. Yu, N. Kees, C. Zheng, *et al.*, "Design and optimization of 99% CEC efficiency soft-switching photovoltaic inverter," in *Applied Power Electronics Conference and Exposition (APEC), 2013 Twenty-Eighth Annual IEEE, 2013*, pp. 946-951.
- [21] W. Yu, J. S. Lai, and S. Y. Park, "An Improved Zero-Voltage Switching Inverter Using Two Coupled Magnetics in One Resonant Pole," *IEEE Transactions on Power Electronics*, vol. 25, pp. 952-961, 2010.
- [22] A. Reibel, "Little Box Challenge Technical Approach Document," 2015.